The Influence of Interannual and Decadal Indo-Pacific Sea Surface Temperature Variability on Australian Monsoon Rainfall

HANNA HEIDEMANN,[a,b] JOACHIM RIBBE,[b] TIM COWAN,[a,c] BENJAMIN J. HENLEY,[d,e,f] CHRISTA PUDMENZKY,[a,b] ROGER STONE,[a] AND DAVID H. COBON[a]

[a] *Centre for Applied Climate Sciences, University of Southern Queensland, Toowoomba, Queensland, Australia*
[b] *School of Sciences, Faculty of Health, Engineering and Sciences, University of Southern Queensland, Toowoomba, Queensland, Australia*
[c] *Bureau of Meteorology, Melbourne, Victoria, Australia*
[d] *School of Earth, Atmosphere and Environment, Monash University, Clayton, Victoria, Australia*
[e] *Department of Infrastructure Engineering, University of Melbourne, Parkville, Victoria, Australia*
[f] *ARC Centre of Excellence for Climate Extremes, Monash University, Clayton, Victoria, Australia*

(Manuscript received 1 April 2021, in final form 25 October 2021)

ABSTRACT: Monsoonal rainfall in northern Australia (AUMR) varies substantially on interannual, decadal, and longer time scales, profoundly impacting natural systems and agricultural communities. Some of this variability arises in response to sea surface temperature (SST) variability in the Indo-Pacific linked to both El Niño–Southern Oscillation (ENSO) and the interdecadal Pacific oscillation (IPO). Here we use observations to investigate unresolved issues regarding the influence of the IPO and ENSO on AUMR. Specifically, we show that during negative IPO phases, central Pacific (CP) El Niño events are associated with below-average rainfall over northeast Australia, an anomalous anticyclonic pattern to the northwest of Australia, and eastward moisture advection toward the date line. In contrast, CP La Niña events (distinct from eastern Pacific La Niña events) during negative IPO phases drive significantly wet conditions over much of northern Australia, a strengthened Walker circulation, and large-scale moisture flux convergence. During positive IPO phases, the impact of CP El Niño and CP La Niña events on AUMR is weaker. The influence of central Pacific SSTs on AUMR has been stronger during the recent (post-1999) negative IPO phase. The extent to which this strengthening is associated with climate change or merely natural internal variability is not known.

KEYWORDS: Australia; Atmosphere-ocean interaction; ENSO; Monsoons; Pacific decadal oscillation; Rainfall; Sea surface temperature; Climate variability; Decadal variability

1. Introduction

Air–sea interactions are a persistent driver of monsoon variability across the globe (Wang et al. 2017). With more than half of the world's population impacted by monsoons (McGregor and Nieuwolt 1998), community livelihoods are tightly linked to monsoonal rainfall (Webster et al. 1998). Having a secure and reliable water resource is critical for agricultural productivity in water-limited or highly variable rainfall regions across the world, such as in the U.S. Midwest (Mehta et al. 2013), northern Australia's tropical and semiarid grazing regions (Cobon et al. 2009), the Mongolian plateau (Lu et al. 2021), and sub-Saharan Africa (Conway et al. 2009). The Australian monsoon (AUM) is a significant source of annual rainfall for tropical northern Australia (Nicholls et al. 1982; Brown et al. 2016) and typically runs from December through March (Davidson et al. 1983; Holland 1986). It is critical for sustaining northern Australia's unique biodiversity and contributing to the region's economic and social prosperity (Suppiah 1992; Bowman 2002).

Climate variability in the tropical and subtropical oceans influences regional monsoon systems on interannual through decadal time scales. On an interannual time scale, El Niño–Southern Oscillation (ENSO) plays a key role in monsoon variability across the globe (Wang et al. 2017). The canonical eastern Pacific (EP) El Niño pattern is associated with warm sea surface temperature anomalies (SSTa) in the central to eastern Pacific Ocean (Rasmusson and Carpenter 1982), while during (typically weaker) central Pacific (CP) events, positive SSTa are located closer to the date line (Ashok et al. 2007). Both EP and CP event types are associated with distinct atmospheric circulations (Timmermann et al. 2018) and regional precipitation patterns (Yuan and Yang 2012). For example, an increase in the frequency of CP El Niño events has led to deficient Indian summer monsoon seasons in recent decades (Srivastava et al. 2019); however, not all extreme El Niño events (which are typically EP events) have led to drought (Kumar et al. 2006) in the same region. La Niña events, which are characterized by cool SSTa in the central and eastern tropical Pacific Ocean (Hoerling et al. 1997), show less diversity than El Niño events, with CP and

Denotes content that is immediately available upon publication as open access.

Supplemental information related to this paper is available at the Journals Online website: https://doi.org/10.1175/JCLI-D-21-0264.s1.

Corresponding author: Hanna Heidemann, hanna.heidemann@usq.edu.au

DOI: 10.1175/JCLI-D-21-0264.1

EP La Niña events being more difficult to distinguish than CP and EP El Niño events (Kug and Ham 2011).

On a decadal time scale, the interdecadal Pacific oscillation (IPO; Power et al. 1999) and its North Pacific manifestation, the Pacific decadal oscillation (Mantua and Hare 2002), influence several monsoon systems. The Pacific decadal oscillation impacts the variability of the East Asian summer monsoon (Si and Ding 2016) and modifies the teleconnections between ENSO and the North American (Carvalho 2020) and South American (Kayano et al. 2020) monsoons. Drought over the West African monsoon region appears to be strongly influenced by the IPO in its positive phase (Rodríguez-Fonseca et al. 2015). The IPO also affects the AUM (Power et al. 1999; Meehl and Arblaster 2011). In addition to decadal variability of the AUM, northwest Australian rainfall has increased during the warmer summer months since the 1950s (Freund et al. 2017). This trend potentially reflects intensified monsoon flow due to external forcings such as aerosols (Dey et al. 2019a) or an increase in the frequency of tropical cyclones and monsoon lows (Clark et al. 2018).

For the AUM, interannual and decadal variability in tropical Pacific SSTa generally has a stronger connection to monsoon rainfall over northeast (NE) than northwest (NW) Australia. The local wind–evaporation feedback sustains the summer monsoon in the NW (Sekizawa et al. 2018). Over consecutive years, soil moisture can be a source of memory for sustaining wet season (November–April) conditions if monsoonal rainfall is low (Sharmila and Hendon 2020). On interannual time scales, ENSO is the most prominent driver of AUM variability (Drosdowsky 1996; Webster et al. 1998), with varying impacts depending on its phase (El Niño or La Niña) and location of maximum SSTa (CP or EP). The AUM onset is typically delayed, and its retreat earlier than usual during CP El Niño events, despite above-average rainfall in January and February (Taschetto et al. 2009, 2010a). Contrasting rainfall patterns (between January and March) over southeast Australia have been linked to the strength of CP El Niño events: strong events were associated with above-average rainfall, whereas below climatological rainfall occurred during weak events (Freund et al. 2021). In response to EP El Niño events, the lower tropospheric zonal winds over northern Australia, representing the AUM circulation, are generally weaker (Kajikawa et al. 2010). This circulation delays the AUM onset (Evans et al. 2014) and leads to relatively drier summer (December–February) conditions over northern Australia. While more extreme EP El Niño events do not necessarily lead to greater northern Australian summer rainfall deficits, rainfall does increase significantly in response to stronger La Niña events (Chung and Power 2017). La Niña events can also reinforce the AUM circulation (Kajikawa et al. 2010), leading to an earlier AUM onset (Evans et al. 2014). Although there is no consensus on a distinction between CP and EP La Niña, CP La Niña events are generally associated with significantly above average summer rainfall over NE Australia (Song et al. 2017). Regional differences in autumn rainfall patterns are associated with CP and EP La Niña (Cai and Cowan 2009).

It has been well established that the IPO is associated with the relationship between ENSO and Australian rainfall (Power et al. 2006), including Australian monsoon rainfall (AUMR; Cai et al. 2010; Meehl and Arblaster 2011). Since the late 1990s, the AUM circulation has strengthened (Kajikawa et al. 2010), accompanying a change of the IPO to its cool phase (negative IPO), and also accompanied by more La Niña events (Choi et al. 2016). While the frequency of CP El Niño events has increased in the last few decades (Yeh et al. 2009; Freund et al. 2019), the influence of different types of ENSO events on AUMR against the backdrop of shifts in the IPO is not yet well understood.

This study analyses the decadal modulation of ENSO's impact on AUMR, using observational and reanalysis data from 1920 to 2020. It distinguishes between canonical EP El Niño/La Niña and CP El Niño/La Niña events. In identifying the mechanisms behind AUMR anomalies during selected events, our study also examines the related large-scale atmospheric circulation and moisture fluxes through a composite approach. The central research question to be answered is this: How does the AUMR response to CP and EP El Niño/La Niña events vary with the phase of the IPO? Our study provides new insights into decadal-scale variability of the interannual relationship between AUMR and tropical Indo-Pacific SSTa.

2. Data and methods

a. Data

Extended austral summer season [December–March (DJFM)] rainfall over northern Australia was analyzed using gridded data from the Australian Water Availability Project (AWAP). AWAP was derived from quality-controlled in situ observations and interpolated onto a 0.05° × 0.05° grid (Jones et al. 2009). The monsoon season of a particular year refers to January–March and December of the preceding year. Due to the lack of observations in central Australia, data in the region 18°–34°S, 121°–134°E were masked out (e.g., Chung and Power 2017). Global sea surface temperature (SST) data with a 1° resolution were obtained from the Hadley Centre Global Sea Ice and Sea Surface Temperature (HadISST) v1.1 dataset (Rayner et al. 2003). SST and rainfall data analysis was restricted from January 1920 to March 2020 due to the uncertainties and limitations of the SST data before 1920 (e.g., Freund et al. 2019). The atmospheric circulation is represented by global mean sea level pressure (MSLP), zonal and meridional winds, and specific humidity from the surface to 300 hPa. These 1°-resolution data were taken from the Twentieth Century Reanalysis version 3 (20CRv3; Slivinski et al. 2019) from 1920 to 2015.

b. Method

AUMR characteristics were evaluated using the total accumulated rainfall over DJFM. Statistical significance is reported at a 5% significance level. AUMR was tested for normality by computing probability density functions (see Fig. 1 in the online supplemental material) and applying the

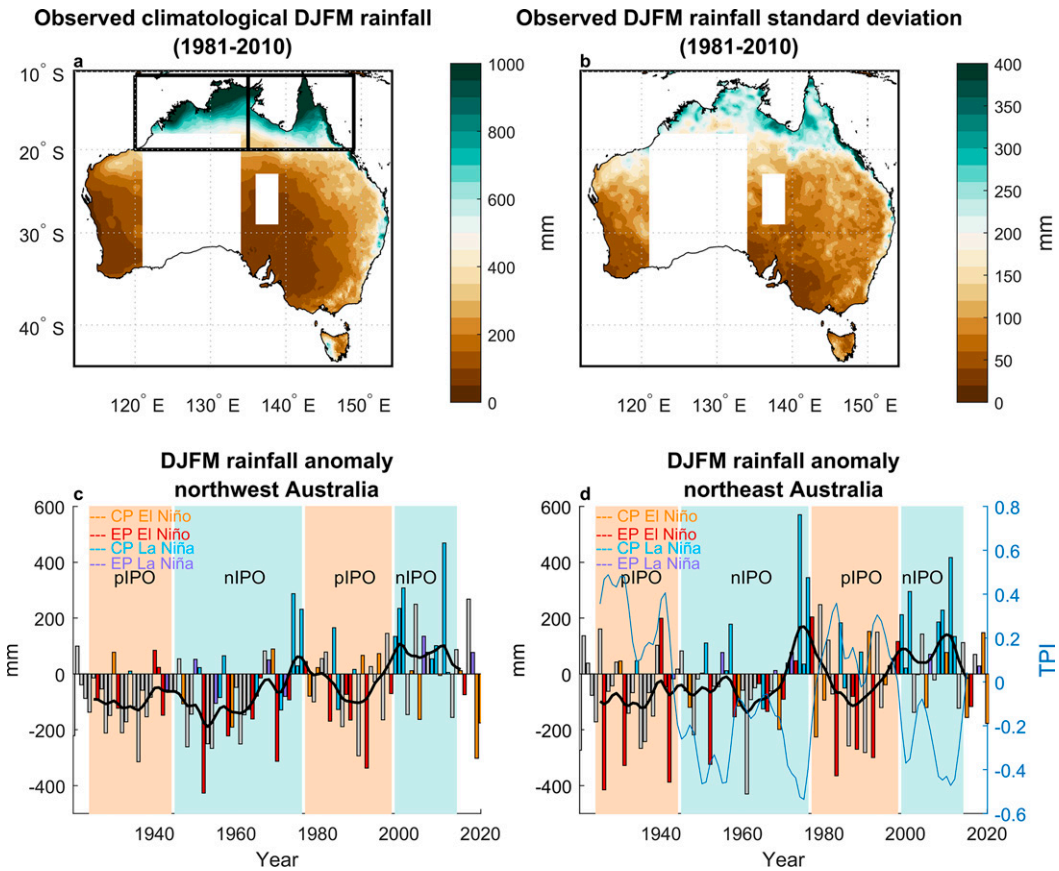

FIG. 1. (a) Climatological Australian monsoon season (December–March) rainfall for the base period (1981–2010). The black box marks the study area. (b) Standard deviation of monsoon season rainfall over Australia for the base period. Data are masked out in central Australia due to the lack of observations (Dey et al. 2019b). Also shown are monsoon season rainfall anomalies for (c) northwest and (d) northeast Australia between 1920 and 2020. Years in which CP El Niño, EP El Niño, CP La Niña, and EP La Niña events occurred are marked in orange, red, blue, and purple, respectively. Decades in which the IPO was in a positive phase are shaded light orange in the background, and negative IPO decades are shaded with a light blue background. The 13-yr low-pass filtered rainfall anomalies are shown as a black line. The 13-yr low-pass filtered IPO Tripole Index (TPI), averaged over DFJM, is shown as a blue line in the background of (d).

Lilliefors test (Lilliefors 1967). In addition, the sample skewness coefficient was calculated (Wilks 2011). To assess the AUMR response to moisture transport via atmospheric circulation anomalies, we used winds and specific humidity to calculate the vertically integrated moisture flux convergence (VIMFC) and integrated zonal and meridional moisture flux (e.g., Taschetto et al. 2009). Rainfall, SSTa, and circulation anomalies were calculated relative to a 1981–2010 climatology and linearly detrended before analysis (except for highlighting trends in Fig. 1). The AUM region is represented by northern Australian land rainfall north of 20°S (see Fig. 1a). Due to the impact of climate drivers on the distribution of rainfall (Risbey et al. 2009; Sharmila and Hendon 2020), the AUM region is also divided along 135°E into a western (NW) and eastern (NE) domain. Rainfall trends were calculated and tested for significance using the nonparametric Mann–Kendall test, as in other studies (e.g., Zhou et al. 2008). The decadal evolution of AUMR since 1920 is highlighted by applying a 13-yr low-pass filter to rainfall (Figs. 1c,d).

1) SST INDICES AND ENSO EVENT DEFINITION

To represent ENSO, we first calculated the Niño-3 (5°N–5°S, 150°–90°W), Niño-4 (5°N–5°S, 160°E–150°W), and El Niño Modoki indices [EMI; determined as in Ashok et al. (2007)]. As the Niño SST indices are highly correlated, they cannot accurately distinguish between different flavors of El Niño (Trenberth and Stepaniak 2001). Furthermore, preliminary results showed that the EMI detected many CP El Niño events before the late 1970s, which differs from other classifications (e.g., Wang et al. 2019). This result shows that the differences in the methods used to separate CP and EP El Niño events can also lead to different results regarding the years classified as a CP or EP event (Capotondi et al. 2015).

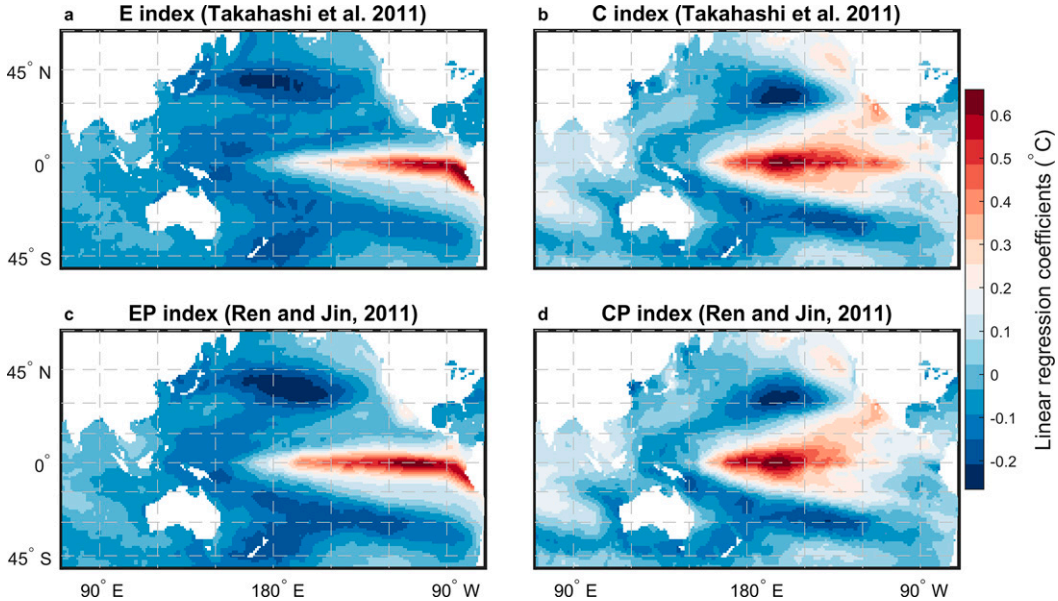

FIG. 2. Linear regression maps showing ENSO indices regressed onto detrended SSTa from 1920 to 2020: (a),(b) E and C indices by Takahashi et al. (2011) and (c),(d) EP and CP indices by Ren and Jin (2011).

Consequently, as in other studies such as Freund et al. (2019), we distinguished between CP and EP El Niño events by computing CP and EP indices following the method of Ren and Jin (2011). CP and EP La Niña events were calculated in the same manner. Before determining ENSO events, the indices were linearly detrended and standardized by subtracting the sample mean and dividing the sample standard deviation.

The C and E indices by Takahashi et al. (2011) were also calculated for comparison and verification purposes. The definitions, threshold criteria, and time series of the Ren and Jin (2011) and Takahashi et al. (2011) indices are shown in Text 2 of the online supplemental material. Regressing the indices of Ren and Jin (2011) and Takahashi et al. (2011) onto SSTa reveals similar spatial patterns (Fig. 2), and the corresponding central and eastern Pacific indices have similar magnitudes and are strongly temporally correlated ($p < 0.001$; see supplemental Fig. 3). To examine the decadal Pacific SST connection to the AUM, we computed the IPO Tripole Index (TPI) and then applied a 13-yr low-pass filter (Henley et al. 2015; see the TPI time series in supplemental Fig. 2). The unfiltered TPI was linearly detrended before calculating correlation coefficients.

2) CORRELATION AND COMPOSITE ANALYSIS

We calculated the Pearson correlation coefficients to explore potential links between global SSTa (75°S and 75°N), including the ENSO SST indices and AUMR variability. These coefficients were also calculated separately for positive and negative IPO epochs (pIPO and nIPO, respectively) from 1924 to 2014, following Henley et al. (2015). The IPO phase between 2015 and 2020 is uncertain due to the nature of low-frequency phenomena and the temporal coverage of the low-pass filters used to measure them. These years were excluded from the decadal analysis, despite a possible shift of the IPO to its positive state around 2014–16 (Meehl et al. 2019). For all correlations, statistical significance was tested using a Student's *t* test.

Teleconnections between Pacific SSTa and AUMR were examined by composite analysis of mean rainfall anomalies during CP/EP El Niño and CP/EP La Niña events. These were specified using the indices by Ren and Jin (2011), and all identified events are summarized in Table 1. The events were examined further during four IPO periods: 1924–44, 1945–76, 1977–98, and 1999–2014. For comparison, ENSO events classified using the C and E indices by Takahashi et al. (2011), along with the associated AUMR and SSTa composites, are shown in supplemental Table 1 and supplemental Figs. 4–6.

The statistical significance of the composited anomalies was determined through Monte Carlo analysis (Boschat et al. 2016; Chung and Power 2017) based on the assumption that the composite data may not be normally distributed (Terray et al. 2003). The Monte Carlo analysis was applied to rainfall, SSTa, and circulation anomalies.

For each month and composite (CP/EP El Niño and CP/EP La Niña, separated by IPO phase), the test statistic $U(X)$ was calculated, which assesses the strength of the departure of the composite anomaly from the overall data mean (Terray et al. 2003):

$$U(X) = (\bar{x}_j - \bar{x})/\sigma_{\bar{x}_j}.$$

At each grid point X, $\bar{x}_j$ is the sample mean of the respective sample group of anomalies (e.g., AUMR anomalies during CP La Niña events within a nIPO phase), $\bar{x}$ is the overall anomaly time series data mean, and $\sigma_{\bar{x}_j}$ is the standard error of the sample mean of the sample group. The null hypothesis for the statistical testing is that the composite anomaly has

TABLE 1. List of eastern Pacific (EP) El Niño and central Pacific (CP) El Niño and La Niña events between 1924 and 2020, as identified using the EP and CP indices by Ren and Jin (2011).

IPO phase (1924–2020)	CP El Niño	EP El Niño	CP La Niña	EP La Niña
pIPO (1924–44)	1929/30	1925/26, 1930/31, 1939/40, 1940/41, 1941/42	1933/34	1942/43
nIPO (1945–76)	1946/47, 1958/59, 1968/69	1951/52, 1957/58, 1963/64, 1965/66, 1969/70, 1972/73, 1976/77	1950/51, 1955/56, 1956/57, 1964/65, 1970/71, 1973/74, 1974/75, 1975/76	1949/50, 1954/55, 1967/68, 1971/72
pIPO (1977–98)	1977/78, 1979/80, 1990/91, 1994/95	1982/83, 1986/87, 1987/88, 1991/92, 1997/98	1983/84, 1984/85, 1988/89, 1998/99	—
nIPO (1999–2014)	2002/03, 2004/05, 2009/10, 2014/15	—	1999/2000, 2000/01, 2007/08, 2008/09, 2010/11, 2011/12	2005/06
IPO? (2015–20)	2018/19, 2019/20	2015/16	—	2017/18
No. of events	14	18	19	7

occurred by chance or lies within the 95th percentile of rainfall anomalies observed between 1920 and 2020.

Second, as many random samples as the number of years included in each composite were selected from the entire anomaly time series 1920–2020 (for each grid point). For example, 14 random samples were selected from the 1920 to 2020 period in the case of CP La Niña events occurring during nIPO phases, for which the same test statistic $U(X)_{\text{random}}$ was calculated. The process was then repeated 1000 times.

Third, the probability density function of these 1000 test statistics $U(X)_{\text{random}}$ was generated. The critical value λ_x was determined at the 5% significance level threshold (2.5th percentile on each end of the distribution). Finally, this critical value needed to be exceeded by the test statistic of the actual data composite $U(X)$ for the null hypothesis to be rejected and the recorded composite anomaly (e.g., for rainfall at a particular grid point) to be considered a significant deviation from the mean of all other anomalies over 1920–2020.

In addition, the false discovery rate (FDR; Benjamini and Hochberg 1995) was calculated for the rainfall composites to detect locations at which the null hypothesis was falsely rejected (Ventura et al. 2004) due to the p value being very close to the threshold of 5%. The FDR helps distinguish between the anomalies' local (p value) and global (FDR) significance. Therefore, a smaller proportion of the locally significant anomalies detected through the above-described process will be FDR (or globally) significant (Ventura et al. 2004). If an anomaly is both locally and FDR significant, this increases confidence. A two-sample t test was used to test the significance of the composite AUMR anomaly differences between nIPO phases and pIPO phases for both the Ren and Jin (2011) (see supplemental Fig. 7) and Takahashi et al. (2011) indices.

3. Results

The following sections explore whether the IPO phase is associated with variability in the teleconnection between AUMR and CP/EP ENSO events. First, section 3a presents the decadal evolution of AUMR during 1920–2020. We then show how correlation coefficients between AUMR and both global SSTa and ENSO indices (section 3b) differ between IPO phases. In section 3c, we analyze ENSO event composites of SST, AUMR, and atmospheric conditions for CP and EP El Niño and La Niña events for both positive and negative IPO phases.

a. Decadal evolution of AUMR and the IPO

Figure 1 shows the climatological mean (μ) and standard deviation (σ) of DJFM rainfall over Australia and a time series of the anomalies averaged over NW and NE Australia. On average, NW Australia experiences lower DJFM rainfall totals than NE Australia (μ_{NW} = 766 mm compared to μ_{NE} = 921 mm; Fig. 1a). Although the NW has a lower standard deviation (σ_{NW} = 218 mm; σ_{NE} = 259 mm), both coefficients of variation (i.e., $\sigma_{\text{NE}}/\mu_{\text{NE}}$ and $\sigma_{\text{NW}}/\mu_{\text{NW}}$) are equal to 0.28. Over the period 1920–2020, NW and NE AUMR show a significant positive trend (16.7 and 15.2 mm decade^{-1}, respectively). An increase in anthropogenic aerosols in the late twentieth century (Rotstayn et al. 2012), the warming in the tropical Atlantic Ocean (Lin and Li 2012), and/or an increase in the occurrence of synoptic events such as tropical cyclones and monsoon lows (Clark et al. 2018) are possible factors in the NW trend. More generally, the positive rainfall trends over northern Australia have also been linked to a warming in the tropical western Pacific (Li et al. 2013) and the recent expansion of the western Pacific warm pool leading to a slowdown in the Madden–Julian oscillation over that region (Roxy et al. 2019).

The decadally smoothed AUMR (for both NW and NE Australia) is lower than the 1981–2010 mean during the first pIPO epoch (1924–44) and most of the nIPO epoch from 1945 to 1976, only becoming above average in the early 1970s (Figs. 1c,d). Coinciding with the shift to the second pIPO epoch (1977–98), AUMR was below average for both regions, where it remained until the most recent nIPO epoch which occurred from 1999 to 2014. During this nIPO, AUMR stayed above the long-term average until the mid-2010s before dipping toward the climatological average, coinciding with a possible return to pIPO conditions (Fig. 1d). Consistent with the

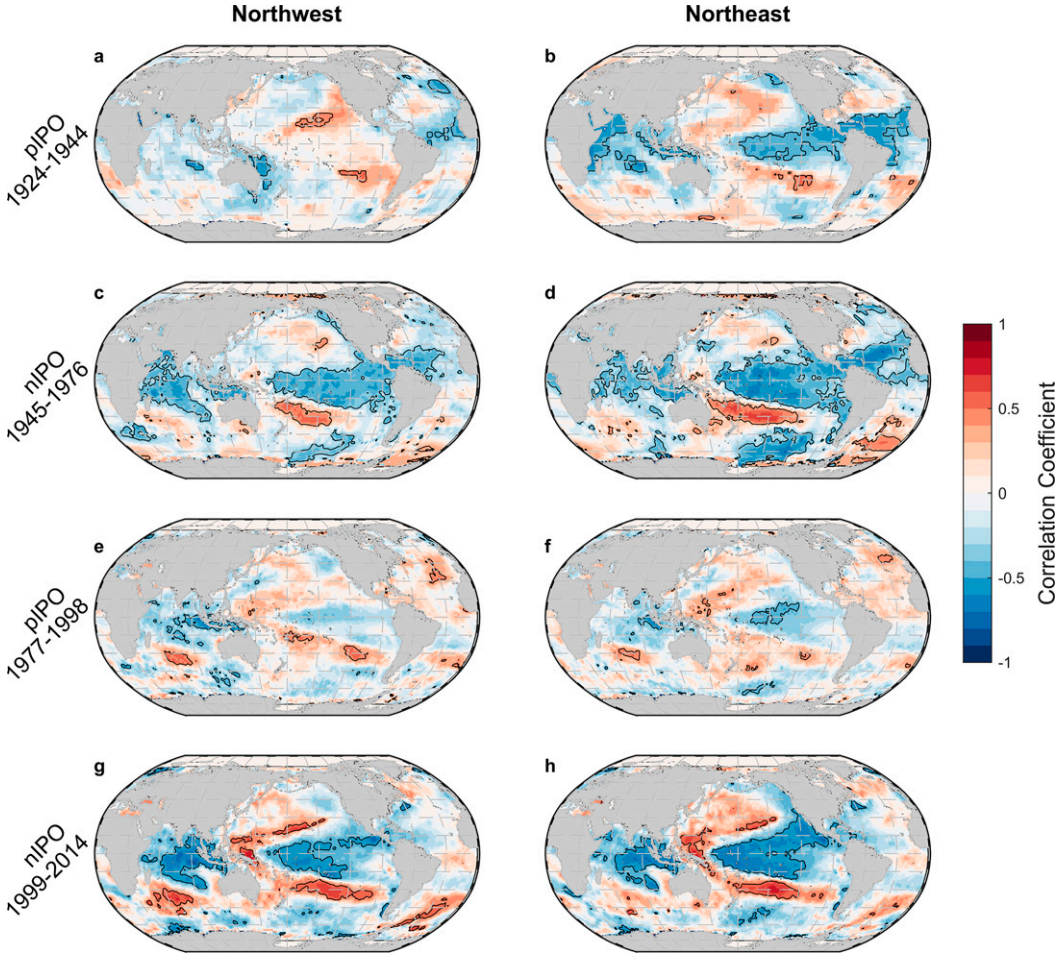

FIG. 3. Correlation coefficients between detrended AUMR anomalies in (a),(c),(e),(g) northwest and (b),(d),(f),(h) northeast Australia and global SSTa, divided into pIPO and nIPO periods from 1924 to 2014. Black contours mark areas of significant correlations at the 5% level using the Student's *t* test.

findings of Sharmila and Hendon (2020), the detrended, unfiltered TPI and AUMR are more strongly anticorrelated over the NE ($R = -0.50$ with $p < 0.05$) than the NW ($R = -0.32$ with $p < 0.05$), indicating that the large decadal variability in AUMR is related to the IPO.

b. IPO-phase dependent SST–AUMR correlations

In this section we examine the correlation coefficient between AUMR and SSTs over the globe, for each IPO epoch (Fig. 3). There are four epochs: one from 1924 to 1944 in which the TPI was predominantly positive, followed by one from 1945 to 1976 in which the TPI was predominantly negative. This is proceeded by another IPO epoch with a predominantly positive TPI from 1977 to 1998 and a last epoch with a negative TPI from 1999 to 2014. Negative correlations in the central-eastern tropical Pacific and positive correlations in the subtropics are visible in all but one IPO epoch, namely 1924–44. This one exception is the NW Australia–related pattern during the first pIPO epoch (Fig. 3a), for which the data are subject to temporal limitations.

During the first pIPO epoch, the NW AUMR–SSTa relationship is primarily weak, with some local significant negative correlations along Australia's eastern seaboard (Fig. 3a). For the same period, the NE AUMR–SSTa correlation pattern resembles a typical La Niña setup, with significant negative correlations in the central-eastern equatorial Pacific Ocean extending into the Atlantic and equatorial Indian Ocean (Fig. 3b). During the following nIPO epoch (1945–76), a stronger La Niña pattern is evident. The pattern includes widespread significant negative correlations over the tropical Indian Ocean and broad positive correlations extending into the subtropical South Pacific Ocean (Figs. 3c,d). As the IPO phase returns positive from 1977 to 1998, the AUMR–SSTa association becomes weaker (i.e., a weak ENSO SST pattern), with rainfall variations showing a stronger coherence to a meridional dipole SST pattern in the equatorial and subtropical Indian Ocean (Figs. 3e,f). During the most recent nIPO epoch (1999–2014), the ENSO-like correlation pattern again strengthens (Figs. 3g,h). Significant correlations in the Pacific Ocean extend beyond the subtropics but not through to the

TABLE 2. Correlation coefficients between detrended Australian monsoon rainfall anomalies and indices for CP El Niño and EP El Niño for IPO phases between 1924 and 2014. Significant correlations at the 5% level are marked with an asterisk.

ENSO index		pIPO (1924/25–1944/45)	nIPO (1945/46–1976/77)	pIPO (1977/78–1998/99)	nIPO (1999/2000–2014/15)
CP index	Northeast	−0.35	−0.60*	−0.27	−0.67*
	Northwest	0.03	−0.43*	−0.16	−0.57*
EP index	Northeast	−0.46*	−0.38*	−0.29	−0.31
	Northwest	0.08	−0.45*	−0.28	−0.31

Atlantic, as seen before the mid-1970s. These results confirm previous findings (e.g., Power et al. 1999), demonstrating the IPO's ability to modulate the relationship between the equatorial Pacific and AUMR on decadal time scales, with the strongest correlations occurring during nIPO epochs. It is also apparent that in the most recent nIPO epoch, the remote forcing on AUMR from the eastern Pacific has weakened (compared to the first nIPO), with a stronger influence stemming from the central tropical Pacific. A novel finding here, which is only possible due to the ∼20 years of observed data after 2000, is that the two nIPO phases of the instrumental era show consistent AUMR–SSTa teleconnection patterns.

Next, we investigate the influence of CP and EP ENSO on AUMR and assess the variability of this relationship between the IPO phases (Table 2). The CP index is more strongly correlated to NE AUMR during nIPO phases (mean $R = -0.62$, $p < 0.05$) than during pIPO phases (mean $R = -0.30$, $p > 0.05$). Also, during these nIPO phases, the influence of the EP index is weaker, which is consistent with the correlation patterns in Fig. 3. Both CP and EP indices are more strongly correlated to NW AUMR during nIPO epochs than during pIPO epochs. The central Pacific influence on AUMR anomalies is stronger in the NE than in the NW (e.g., Sekizawa et al. 2018; Sharmila and Hendon 2020). When comparing the most recent and earlier nIPO epochs, the correlation between the CP index with both NW and NE AUMR increases (implying a stronger relationship), while the correlation between the EP index and both NW and NE AUMR decreases (inferring a weaker relationship). The emerging central Pacific influence might relate to the observed warming trend in the western Pacific and associated intensification of the meridional SST gradient, which increases the likelihood of warm SSTa in the Niño-4 region (Wang et al. 2019). This emerging influence is consistent with a shift from more frequent moderate EP El Niño events to moderate CP El Niño events after the late 1970s, in addition to more strong basinwide El Niño events that also originate in the western Pacific (Wang et al. 2019).

c. *Seasonal and monthly ENSO–AUMR association*

In the following subsections (1–5), we compare how the IPO phase influences the SSTa patterns during CP/EP El Niño and CP/EP La Niña events, the ENSO–AUMR teleconnection and discuss observed mechanisms in section 3c(7). This comparison is made analyzing the IPO phase-dependent contrast in the ENSO–AUMR correlations, which shows that AUMR is affected by both ENSO event type and IPO phase. Note that the case of EP La Niña events in pIPO phases is omitted due to only one event occurring. The AUMR composites were also replicated using the Takahashi et al. (2011) ENSO indices (see supplemental Text 2) and are compared to the AUMR composites using the Ren and Jin (2011) ENSO indices in section 3c(6).

1) SSTA COMPOSITES

We observed a peak in the warm SSTa across the central Pacific for CP El Niño events in pIPO phases. Anomalously cool SSTs lie to the north of Australia and extend through to the western Pacific warm pool area, but not beyond the Indonesian Throughflow region (Fig. 4a). During nIPO phases, the warm SSTa over the central Pacific are more widespread, yet the cool SSTa to the north of Australia weaken (Fig. 4b). The warm Pacific SSTa shift to the central (east of the date line) and eastern regions for EP El Niño events during pIPO phases (Fig. 4c). Significant cool SSTa across the central subtropical-to-midlatitudes in the North Pacific and cool SSTa south of the Niño regions are reminiscent of the climatological conditions during the most recent pIPO epoch (Henley et al. 2015). A striking difference in the regions of absolute SST maxima between CP and EP El Niño events is observed regardless of the IPO phase. The SST maximum during EP El Niño events is near the date line. In contrast, the maximum during CP El Niño events occupies a much larger area stretching from the western Pacific throughout the central Pacific (approximately 150°E–160°W; see supplemental. Fig. 8). Another important difference between the EP and CP El Niño composites during pIPO phases is the extensive warm SSTa across the tropical Indian Ocean that resembles the basinwide warming pattern (Taschetto et al. 2011). This pan-Indian Ocean warming and off-equatorial Pacific cool SSTa are largely absent during EP El Niño events in nIPO phases. The meridional extent of the equatorial Pacific warm SSTa is also substantially narrower, confined to ∼15° off the equator (Fig. 4d). Upon inspection of the month-to-month variability (not shown), there is a considerable weakening of the warm SSTa by February and March, with earlier termination of El Niño in nIPO phases than observed during pIPO phases. Considering La Niña event types, there are key differences in the composite patterns associated, particularly with CP La Niña events, across the two IPO phases. These include the broader cool SSTa that extend farther in the far eastern Pacific, meridionally along the west coast of North America and westward into the tropical Indian Ocean during nIPO phases (Fig. 4f). In contrast, the cool SSTa are noticeably more equatorially trapped in the central to eastern Pacific during pIPO phases

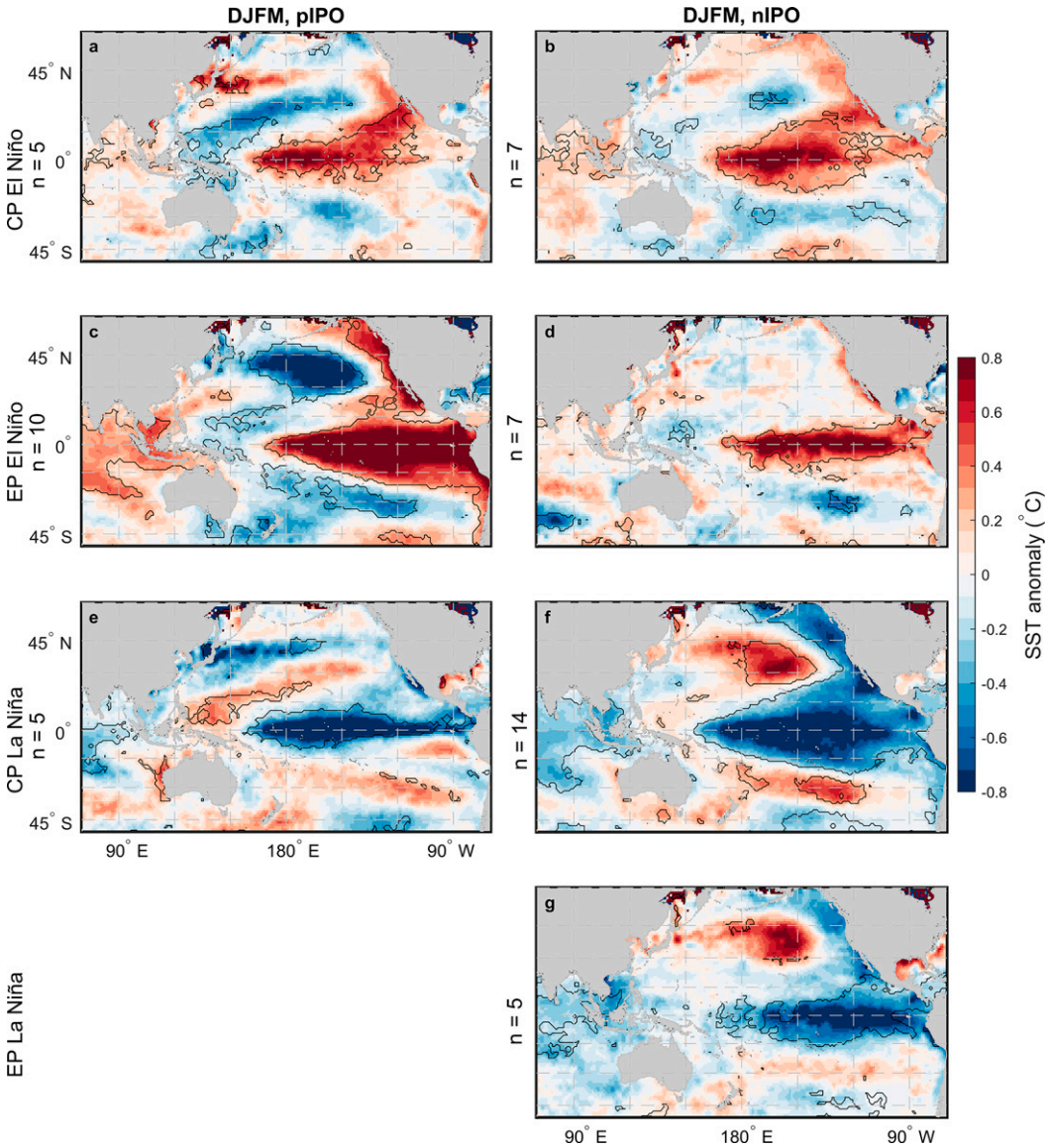

FIG. 4. Detrended SSTa composites for the AUM season showing the large-scale SSTa in the Pacific and the eastern Indian Ocean during (a),(b) CP El Niño, (c),(d) EP El Niño, (e),(f) CP La Niña, and (g) EP La Niña events as identified using the CP and EP indices by Ren and Jin (2011); during (left) pIPO and (right) nIPO phases from 1924 to 2014. Black contours mark areas with significant anomalies at a 5% level based on the Monte Carlo method.

(Fig. 4e). Another major difference, seen only during pIPO phases, is the warm SSTa along Australia's west coast and the southern Philippine Sea. As shown earlier, these regional SSTa are only weakly associated with AUMR over the NE AUM region during the most recent IPO phase (Fig. 3f). Despite the low number of sampled events, the associated SSTa composites during EP La Niña events show similar patterns during nIPO phases (Fig. 4g). However, the spatial extent of the cool SSTa around the equatorial Pacific is smaller than for CP La Niña events.

In the following sections, the seasonal and subseasonal AUMR composites for these ENSO events, separated into pIPO and nIPO phases, are analyzed (Figs. 5 and 6, respectively).

2) CP EL NIÑO

During CP El Niño events in pIPO phases, AUMR decreases in December and March and increases in January and February over much of northern Australia (Figs. 5a,d,g,j). In February, significant positive anomalies cover nearly all NW Australia, but this flips in March to widespread negative anomalies across northern Australia, predominantly significant over the NE. The positive AUMR anomalies in the NW in January and February dominate the overall DJFM total, with AUMR 3% above average over northern Australia during pIPO phases (Fig. 5m). During nIPO phases, total DJFM AUMR is 8% below the climatology over northern Australia,

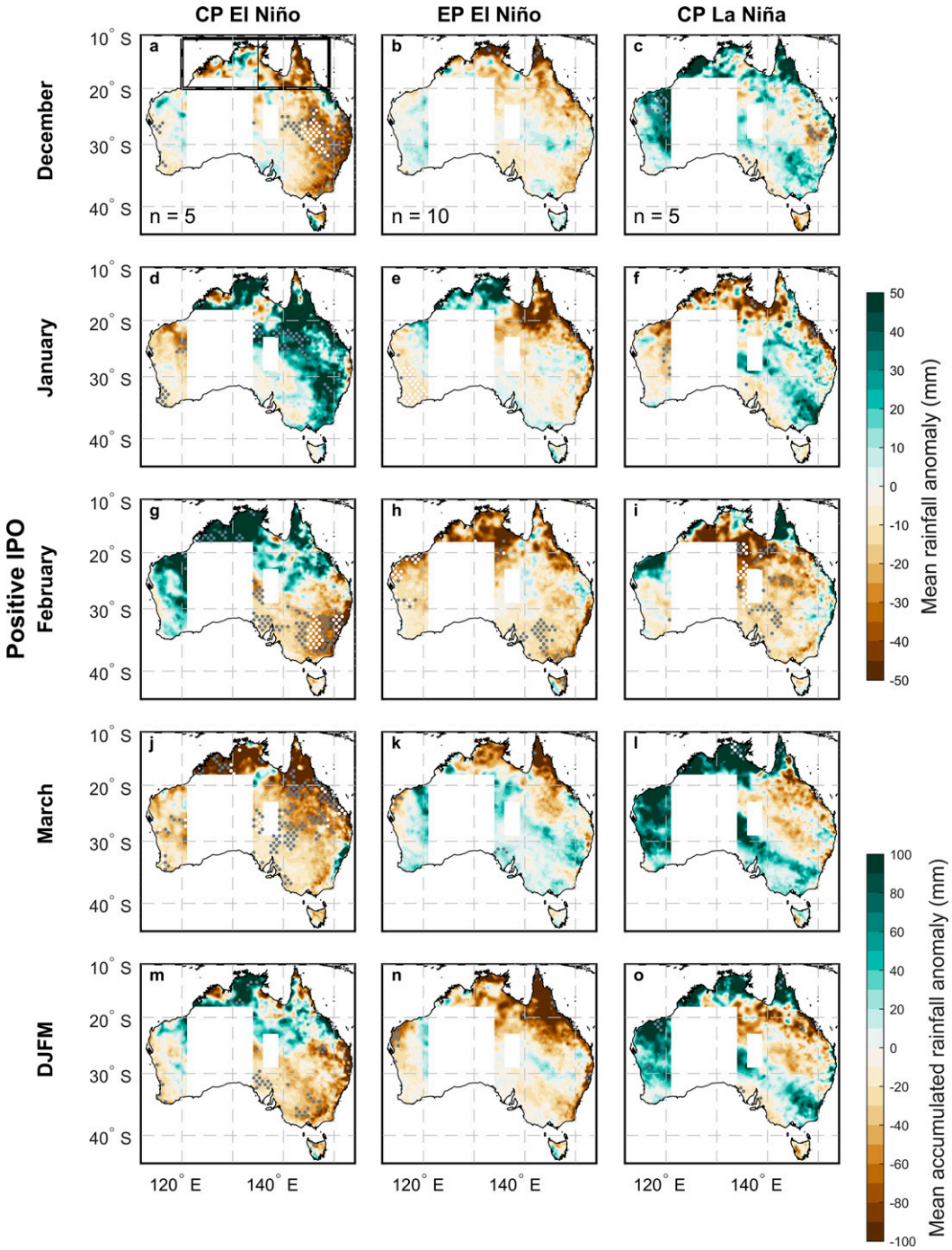

FIG. 5. Detrended AUMR anomaly composites in pIPO phases between 1924 and 2014 for (left) CP El Niño, (center) EP El Niño, and (right) CP La Niña events as identified using the CP and EP indices by Ren and Jin (2011). Significant anomalies at a 5% level using the p value based on the Monte Carlo method are marked with gray stippling. The false discovery rate at a 5% level is marked with white stippling.

influenced strongly by significant negative anomalies in the far northeast Cape York region (Fig. 6q). The seasonal anomalies reflect the pattern observed in February; outside of Cape York for this month, AUMR anomalies are mostly weak and insignificant (Figs. 6a,e,i,m). The most significant AUMR anomaly differences between the IPO phases were observed in February (see supplemental Fig. 7). Due to the increased frequency of CP El Niño events since the late 1970s (e.g.,

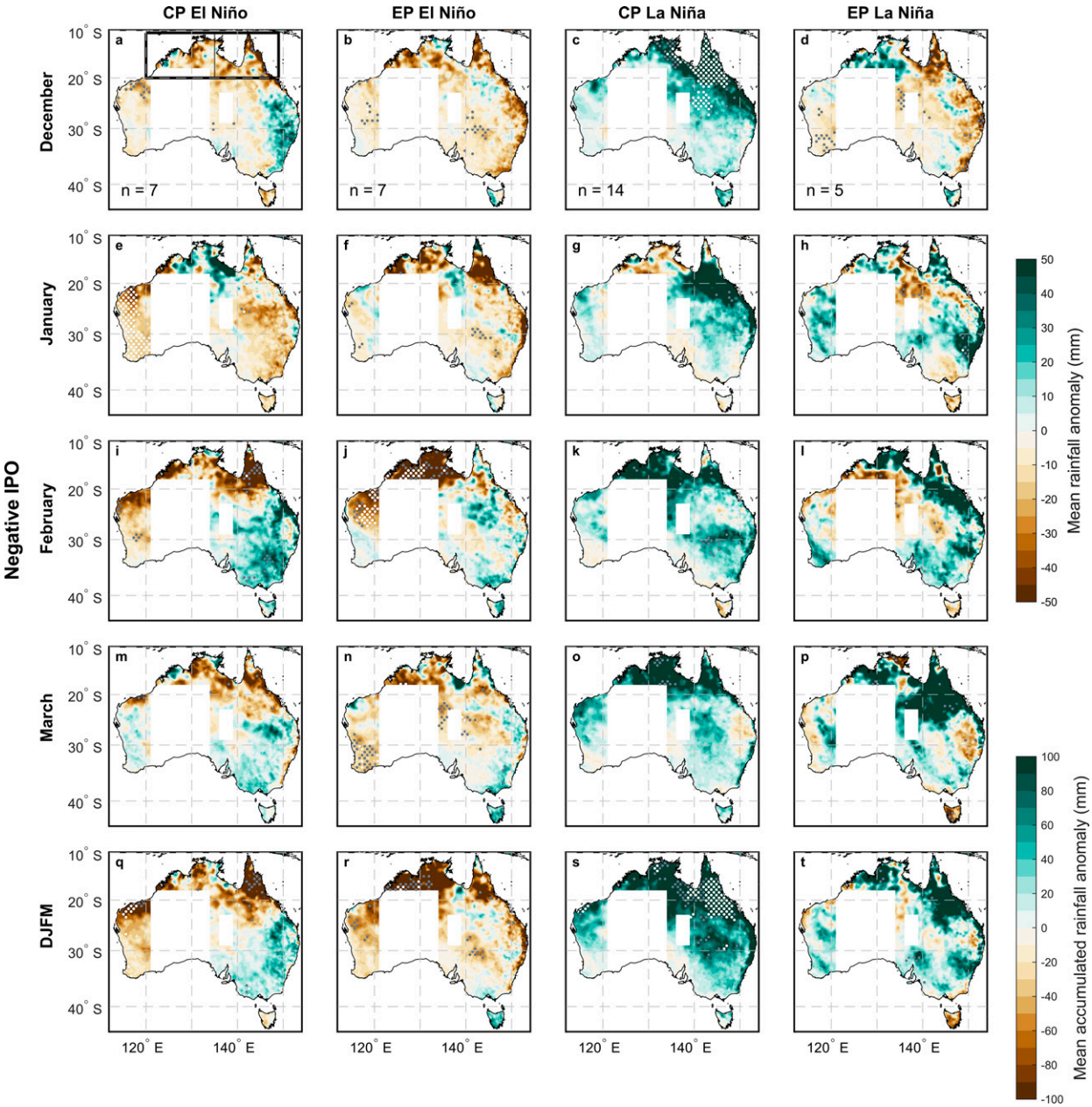

FIG. 6. As in Fig. 5, but for nIPO phases, and including EP La Niña events.

Freund et al. 2019), the composites mainly reflect events in the more recent IPO phases (see Table 1) and, subsequently, the response in AUMR to these events in the 1980s and 1990s (i.e., coinciding with a pIPO background state).

3) EP EL NIÑO

The monthly and total DJFM AUMR anomaly composite patterns associated with EP El Niño events indicate drier than average conditions (in both IPO phases) across most of northern Australia, except for a wetter than average (not significant) NW in January (pIPO phase composites in Figs. 5b,e,h,k,n; nIPO composites in Figs. 6b,f,j,n,r). The most significant negative rainfall anomalies are found over the NE in January and over the NW in February (Figs. 5fe,h and 6f,j, respectively). The frequency of EP El Niño events has decreased in recent decades, with only one EP event since 2000, in 2015/16 (Table 1; as of February 2021). Ten of the 17 EP El Niño events have occurred during pIPO phases, during which the total DJFM rainfall over the NE was 17% below average, with weak anomalies over the NW (Fig. 5n). Despite the anomalously dry conditions that persist across the summer months, the rainfall anomalies are insignificant. The remaining

seven EP El Niño events all emerged within the 1945–76 nIPO phase, during which the total DJFM rainfall anomaly was 13% below average over the NW (Fig. 6r). As with CP El Niño events (Fig. 6i), the most significant rainfall anomalies for EP El Niño events during nIPO phases occur in February (Fig. 6j). In this month, significant negative rainfall anomalies are a feature over NW Australia. It can be noted that the FDR shows a significant effect as well (Fig. 6j). In general, AUMR tends to be below average over northern Australia (and for individual months) during EP El Niño events regardless of the IPO phase, a finding consistent with previous research (e.g., Risbey et al. 2009; Chung and Power 2017). The presence of stronger anomalies over the NE under pIPO conditions and over the NW under nIPO conditions suggests that the background Pacific state has an association with the spatial distribution of the negative AUMR anomalies associated with El Niño.

4) CP La Niña

Most La Niña events are classified as CP events. Fourteen out of 19 events occurred during nIPO phases, giving rise to significantly above average (20%) DJFM rainfall over northern Australia (Fig. 6s). While positive rainfall anomalies over northern Australia appear in all months, they are only significant over NE Australia in December (supported by the FDR) (Figs. 6c,g,k,o). Therefore, December is when La Niña appears to have the strongest impact on rainfall over NE Australia, whereas February is when the IPO phase appears to have the greatest influence on AUMR (i.e., the difference between nIPO and pIPO phases; see supplemental Fig. 7). Only observing five CP La Niña events in pIPO phases limits our ability to draw robust conclusions. Over much of northern Australia, negative rainfall anomalies are observed in January and February (Figs. 5f,i). Despite this, total DJFM AUMR is above average in the far northern region but mostly insignificant (Fig. 5o) and much weaker than during nIPO phases. The significant positive anomaly in total DJFM AUMR during CP La Niña events in nIPO phases occurs more widely than DJFM anomalies during any other type of ENSO event. In the analyzed period from 1920 to 2020, this CP La Niña and nIPO combination has coincided with historical record-breaking wet summers over northern Australia, including the early 1970s as well as 2011 (see Figs. 1c,d).

5) EP La Niña

EP La Niña events are much less common than CP La Niña events during each IPO phase (Table 1), in agreement with the number of events classified using the Takahashi et al. (2011) ENSO indices (see supplemental Table 1). The majority (5 out of 6) of EP La Niña events have occurred during nIPO phases, and an above-average (8%) response in DJFM AUMR over northern Australia with positive anomalies stretches down into southeast coastal Queensland (Fig. 6t). The rainfall anomalies across the season (and total) are mostly insignificant, aside from southeast Queensland in December and central New South Wales in January (Figs. 6d,h,l,p). During pIPO phases, the extremely small sample size of only one EP La Niña event makes it impossible to evaluate the typical rainfall patterns associated with these events. In summary, during EP La Niña events, above-average rainfall occurs in the late monsoon season months in nIPO phases, whereas rainfall patterns during pIPO phases are uncertain due to so few events.

6) Comparison between AUMR composites using the Ren and Jin (2011) and Takahashi et al. (2011) indices

Even though the number of ENSO events identified through the method by Takahashi et al. (2011) differs from the events determined using the Ren and Jin (2011) indices, the composite AUMR anomaly patterns are generally consistent (see Figs. 5 and 6 and supplemental Figs. 4 and 5). The total DJFM AUMR composites show the strongest agreement during nIPO phases for CP El Niño and CP La Niña events. The events classified using both methods are identical for CP La Niña events in pIPO phases. In contrast, for nIPO phases, Takahashi et al. (2011) detect two additional events, yet the rainfall composites remain almost identical, giving a high degree of confidence in our CP La Niña results. The most substantial differences between the Ren and Jin (2011) and Takahashi et al. (2011) definitions are found for EP El Niño events in January during nIPO phases (not shown). For these events, the definition using the Ren and Jin (2011) indices captures seven events during pIPO phases, while the Takahashi et al. (2011) indices capture five events, which are all included in the events classified using the Ren and Jin (2011) indices. Therefore the rainfall anomalies during the two additional events with Ren and Jin (2011) indices have smoothed out the strong positive rainfall anomalies over the NW, which were observed in EP El Niño events in January using the Takahashi et al. (2011) indices (see supplemental Fig. 4). These sample size differences lead to the differences over the NW during pIPO phases between the two definitions.

7) Mechanisms

We now focus on the differences in the large-scale anomalous atmospheric circulation associated with CP El Niño/La Niña, where we concentrate on the month in which the AUMR anomalies are the strongest. Figure 7 displays the MSLP and 850-hPa wind anomalies during pIPO and nIPO phases for the CP events, averaged across DJFM (Figs. 7a,c,e,g), and for El Niño events in February (Figs. 7b,d) and La Niña events in December (Figs. 7f,h). Circulation anomalies for each month, ENSO state, and IPO phase are included in supplemental Figs. 9 and 10. We also analyze anomalies of VIMFC and zonal and meridional components of vertically integrated moisture fluxes for the same events (Fig. 8). Note that repeating this analysis with trends included leads to similar composites and does not change the results.

(i) CP El Niño

The DJFM surface conditions during CP El Niño events in pIPO phases consist of an anomalous high pressure center over the Maritime Continent (i.e., western North Pacific anticyclone) and negative MSLP anomalies over the central

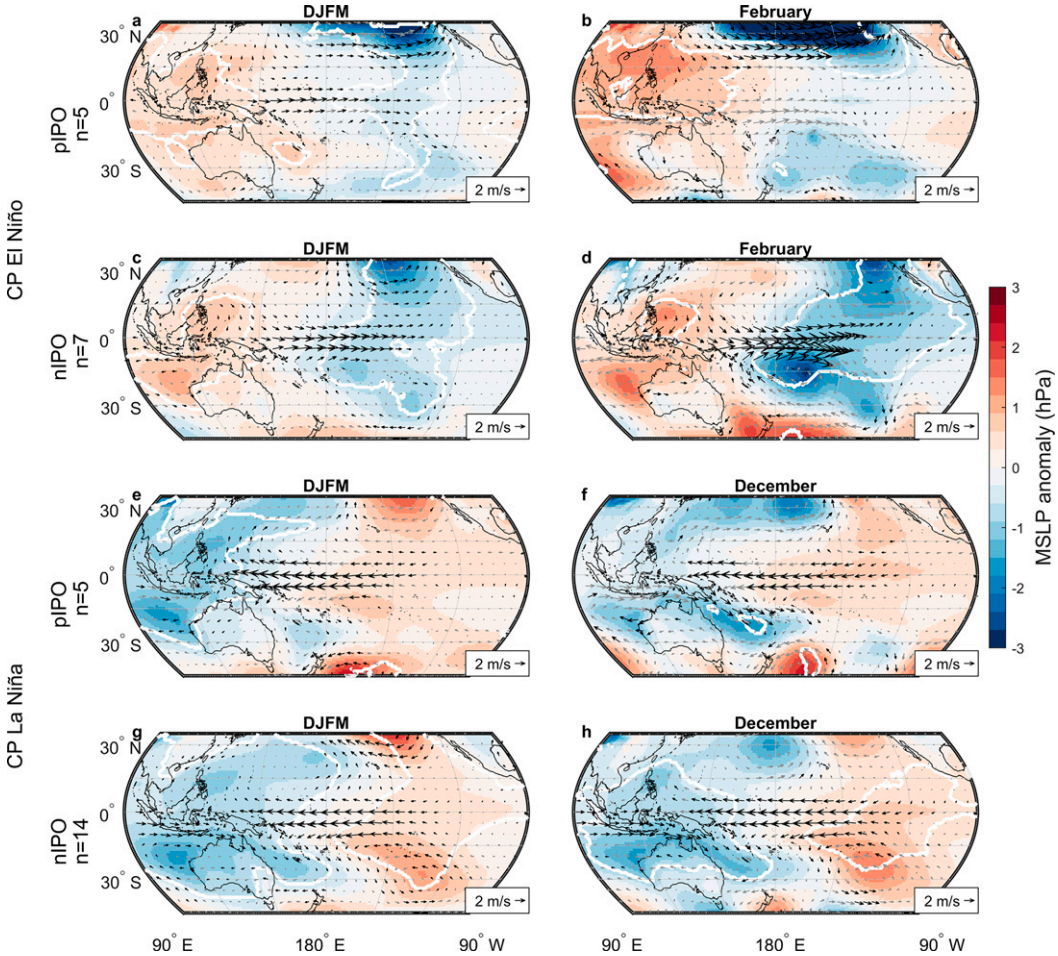

FIG. 7. Detrended MSLP (shading) and 850-hPa wind (vectors) anomaly composites for selected events. CP El Niño composites are shown for (a),(b) pIPO and (c),(d) nIPO phases from 1924 to 2014 averaged (a),(c) across DJFM and (b),(d) in February. Also shown are CP La Niña composites during (e),(f) pIPO and (g),(h) nIPO phases averaged (e),(g) across DJFM and (f),(h) in December. White contours mark areas with significant MSLP anomalies, and black vectors indicate significant wind anomalies at a 5% level based on the Monte Carlo method.

Pacific. This setup supports westerly wind anomalies at 850 hPa over the western equatorial Pacific (Fig. 7a).

In February, the anomalous anticyclone in the western Pacific is particularly strong as El Niño decays (e.g., Stuecker et al. 2015), yet the pressure gradient across the equatorial west Pacific is weak, and wind anomalies are insignificant. Anomalous westerlies across NW Australia arise due to a weak anomalous cyclonic circulation (Fig. 7b), locally advecting moisture into the region (Fig. 8b). This local cyclonic circulation, which relates to the strengthening of the South Pacific convergence zone (SPCZ) via deep convection in the western-central Pacific (e.g., Taschetto et al. 2010a), dominates the AUMR response leading to increased rainfall (Fig. 5g).

For CP El Niño events in nIPO phases, there are noticeable differences in MSLP and the low-level wind anomalies, although the surface pressure pattern in DJFM broadly resembles that for pIPO phases. These differences include a westward and southward extension of significant negative MSLP anomalies in the central Pacific and a stronger west-to-central equatorial Pacific zonal pressure gradient. Accordingly, we see stronger anomalous westerlies at 850 hPa along the equator (Fig. 7c), leading to significant moisture flux convergence in the central Pacific (Fig. 8c). Positive MSLP anomalies in the form of a well-defined anticyclonic anomaly are located to the northwest of Australia. These anomalies lead to an eastward shift of the MSLP gradient between the western and central Pacific. The mean-state westerly monsoonal flow is weakened over NW Australia and the Timor Sea to the north, and the westerlies to the northeast of Australia strengthen (Fig. 7c). The flow subsequently leads to strong moisture flux divergence over northern Australia and the adjacent oceans (Fig. 8c).

It appears that February dominates the conditions in DJFM during nIPO periods, showing the strongest MSLP and 850-hPa wind anomalies in comparison to the other months

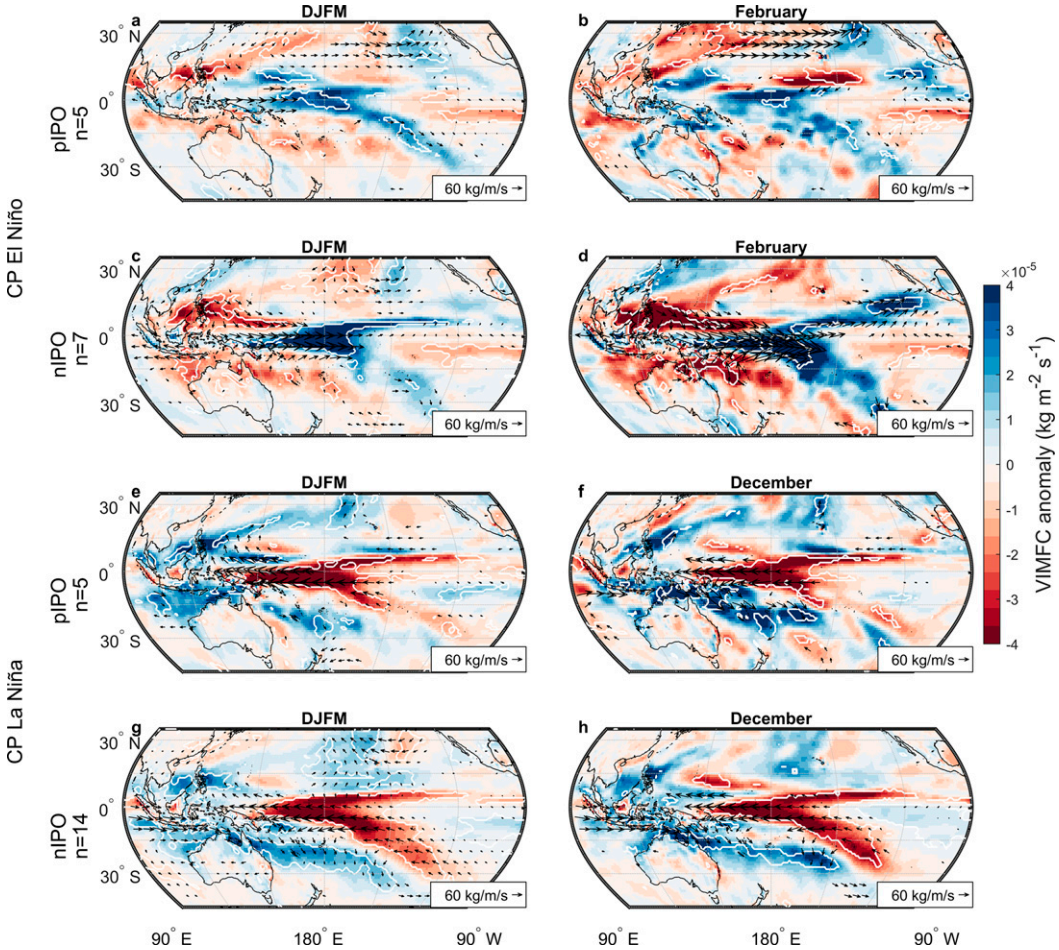

FIG. 8. Detrended vertically integrated moisture flux convergence (VIMFC; shading) and zonal and meridional components of vertically integrated moisture flux (vectors) anomaly composites for selected events. CP El Niño composites are shown for (a),(b) pIPO and (c),(d) nIPO phases from 1924 to 2014 averaged (a),(c) across DJFM and (b),(d) in February. Also shown are CP La Niña composites during (e),(f) pIPO and (g),(h) nIPO phases averaged (e),(g) across DJFM and (f),(h) in December. White contours mark areas with significant anomalies at a 5% level based on the Monte Carlo method. Positive values indicate convergence, while negative values indicate divergence of moisture fluxes. Moisture flux vectors are shown only for significant anomalies at a 5% level based on the same method.

(see supplemental Fig. 10). A canonical strong (negative) Southern Oscillation pattern is evident during this month, characterized by positive MSLP anomalies over northern Australia and negative MSLP anomalies in the central Pacific, accompanied by strong anomalous easterly winds (Fig. 7d). The same anomalous anticyclone is evident off northwest Australia, although it is considerably stronger than the DJFM average (Figs. 7c,d). The VIMFC anomaly indicates divergence over northern Australia and across the oceanic regions northwest and northeast of it, with an anomalous eastward flux and strong convergence of moisture in the central Pacific (Fig. 8d). The strong remote connection between the Maritime Continent and the equatorial Pacific helps to explain the dry conditions over Australia's monsoon region during February in nIPO phases (Fig. 6i).

(ii) CP La Niña

During CP La Niña events in pIPO phases, the DJFM average shows anomalous easterlies in the western equatorial Pacific, associated with a zonal MSLP gradient and positive pressure anomalies throughout the Western Hemisphere (Fig. 7e). An anomalous cyclonic circulation off Australia's northwest coast reinforces the climatological westerly monsoon flow from Sumatra/Java to NW Australia (Fig. 7e), leading to anomalous moisture convergence there (Fig. 8e). A large region of significantly negative pressure anomalies is located west and northwest of Australia (Fig. 7e). Weakly anomalous moisture convergence east of Australia indicates the approximate location of the SPCZ. Owing to its position off the Australian east coast, the SPCZ has little influence on rainfall over eastern Australia (Fig. 8e).

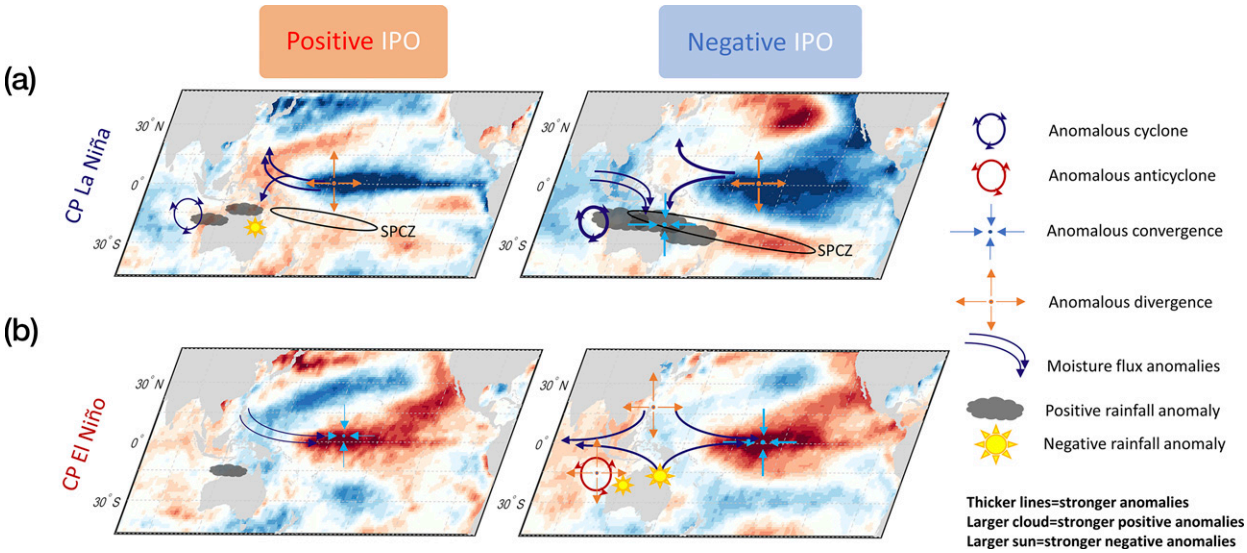

FIG. 9. Schematic summarizing DJFM AUMR anomalies and atmospheric features associated with (a) CP La Niña and (b) CP El Niño events during (left) pIPO and (right) nIPO phases. SSTa are shown in the background of each panel. The approximate location of anomalous cyclones and anticyclones is indicated, as well as the direction of anomalous moisture fluxes and regions of moisture flux convergence and divergence.

In December, negative pressure anomalies in the Coral Sea coincide with strong moisture convergence anomalies stretching from Papua New Guinea past New Caledonia (Figs. 7f and 8f), which indicates the southward displacement and extension of the SPCZ.

In nIPO phases, CP La Niña events are associated with a deep surface trough extending across northern Australia, a significant feature over the entire Indo-Australian region. As in pIPO phases, an anomalous cyclone is located in the eastern tropical Indian Ocean and the Coral Sea, which is now characterized by significant cyclonic wind anomalies (Fig. 7g). Strong anomalous westerlies along the northern flank of the cyclone anomaly off NW Australia indicate enhanced monsoonal flow toward northern Australia (Fig. 7g). Strong anomalous easterlies in the central equatorial Pacific, typically associated with La Niña events, help maintain the negative MSLP anomalies in the western Pacific and the Maritime Continent (Fig. 7g). The cyclonic circulation anomalies and the easterlies result in anomalous moisture transport and convergence over northern Australia (Fig. 8g), driving enhanced monsoon rainfall. The anomalous convergence of moisture over NE Australia, the Coral Sea, and stretching eastward into the southwest Pacific indicates an extension and southwestward displacement of the SPCZ (Fig. 8g).

The December atmospheric conditions associated with CP La Niña events are similar to the DJFM nIPO phase average but show a deeper pressure trough over northern Australia (Fig. 7h). In the following months, January to March, similar MSLP and low-level wind anomaly patterns can be found over northern Australia and the central Pacific. These patterns vary in strength (see supplemental Figs. 10k–n) and favor above-average rainfall over northern Australia (Figs. 6g,k,o). Anomalous moisture convergence in a region including the SPCZ and NE Australia is the strongest and most significant in December (Fig. 8h) compared to January–March (not shown). The convergence can explain the significantly enhanced rainfall over north and NE Australia in December (Fig. 6c), suggesting that the atmospheric anomalies, including the southwestward shift of the SPCZ, are particularly important during the monsoon onset month.

For CP El Niño and La Niña events, the different numbers of sampled events might explain the composite pattern differences between the IPO phases. With a small sample size of five CP El Niño events for pIPO phases, one or two extreme magnitude events can heavily skew any composite pattern. For CP La Niña events, the sample size for nIPO phases (n = 14) is much larger than for pIPO phases (n = 5). Hence the nIPO phase results are more robust than the pIPO phase results.

4. Discussion

This research builds upon previous studies (e.g., Meehl and Arblaster 2011; Klingaman et al. 2013; Choi et al. 2016), which investigated the impacts of ENSO and the IPO on the AUM, with a focus on rainfall. The strongest contrast in AUMR between nIPO and pIPO phases is seen during CP El Niño and CP La Niña events and the weakest during EP El Niño events (see supplemental Fig. 7 for details). It is further shown in detail how AUMR varies during ENSO events depending on the IPO phase. In Fig. 9 the DJFM AUMR anomalies and associated mechanisms during CP El Niño and La Niña events are summarized in a schematic. In the following, we discuss the main decadal differences and similarities in the observed AUMR during ENSO events within the four analyzed IPO epochs.

a. CP El Niño events

The decadal differences in the CP El Niño–AUMR association have not previously been explored. A study by Taschetto et al. (2009) demonstrated that between 1979 and 2005, CP El Niño events were associated with a shorter but intensified AUMR season. The anomalous moisture transport over NW Australia reinforced the climatological conditions, causing increased rainfall in January and February (Taschetto et al. 2010a). This result is consistent with our AUMR composites for CP El Niño events during pIPO phases (Figs. 5a,d,g,j) as well as the low-level anomalous cyclonic circulation near NW Australia in February (Fig. 7b) acting as a moisture source for the region (Fig. 8b).

In contrast, during the same month in a nIPO phase, the negative NE AUMR anomalies (Fig. 6i) and a strong equatorial zonal pressure gradient and anticyclonic circulation off NW Australia (Fig. 7d) differ from previously published results such as those of Taschetto et al. (2009, 2010a,b). There is the possibility that the cool background SSTs (i.e., nIPO phase) partially offset the impact of the warming in the central Pacific on enhancing convection. The inference is that the cooler background SST conditions during nIPO phases may weaken the diabatic heating that causes the Gill–Matsuno-type response in the upper troposphere. Subsequently, the east-to-west equatorial Rossby waves may be too weak or infrequent to trigger a cyclonic circulation over the NW. Taschetto et al. (2010a) identified this Gill–Matsuno-type mechanism and subsequent anomalous cyclone over NW Australia as the cause for above-average rainfall across northern Australia during CP El Niño events. This mechanism and the enhanced AUMR were detected in the peak monsoon months of January and February using targeted SST warming numerical modeling experiments (Taschetto et al. 2010a). The anticyclonic circulation off NW Australia (during a nIPO phase) may also be related to the anomalously cool SST off western Australia, which occur in February (not shown) but can also be detected in the DJFM average (Fig. 4). These negative SSTa are quite weak and insignificant. The underlying mechanism for the strong divergence over northern Australia and moisture flux toward the central Pacific during CP El Niño events in nIPO phases could be further investigated in a future study using numerical model simulations (e.g., Taschetto et al. 2010a).

b. EP El Niño events

The similarity of AUMR anomalies during EP El Niño events between both IPO phases might indicate that AUMR–El Niño anomalies are controlled mainly by interannual variability and less so by the background state conditions. Interestingly, despite the much stronger large-scale VIMFC anomalies across the central and eastern Pacific during pIPO phases than during nIPO phases, the moisture flux divergence anomalies are still insignificant over northern Australia during both IPO phases (not shown). One idea is that AUMR anomalies during EP El Niño events might be more influenced by local SSTa or extensive warm SSTa patterns in the tropical Indian Ocean, driving subsidence over Australia during EP El Niño events (Taschetto et al. 2011).

Another consideration regarding the weak decadal differences in AUMR anomalies during EP El Niño events relates to the overall less substantial effect of El Niño than La Niña events on northern Australian summer rainfall. The nonuniform response of AUMR anomalies to El Niño and La Niña events was explored by Chung and Power (2017). They found a more significant impact of La Niña than El Niño on summer rainfall anomalies over northern Australia. However, their analysis did not focus on the Pacific background state or the different ENSO flavors (CP/EP). Chung and Power (2017) also showed that strong El Niño events were associated with above- and below-average rainfall over NW and NE Australia, respectively (both insignificant). This study includes both weak and strong ENSO events to avoid undersampling in evaluating the composite AUMR anomalies. Our study has expanded on Chung and Power (2017) by 1) confirming that the effect of EP El Niño events on AUMR stays weak in both IPO phases and 2) showing that the impact of CP La Niña events on AUMR is much stronger than the impact of EP El Niño events, but that there is a high degree of decadal variability in the CP La Niña–AUMR teleconnection.

c. CP La Niña

The strong relationship between positive AUMR anomalies and CP La Niña events only exists during nIPO phases through the anomalous convergence of moisture from the Pacific and Indian Oceans, which occurs over NE Australia (Fig. 8g). The IPO phase-related difference in rainfall during La Niña events has previously been shown for other parts of Australia. Contrasting one negative (1950–79) and one positive (1980–2008; note that the period is different from our definition) IPO phase, Cai et al. (2010) attributed the difference in southeast Queensland summer rainfall to a difference in the position of the SPCZ. During the first analyzed period (1950–79, mostly encompassing a nIPO phase), CP and EP La Niña events were associated with above-average rainfall in the region. In contrast, from 1980 to 2008 (predominantly covering a pIPO phase), summer rainfall in southeast Queensland was well below average (Cai et al. 2010) due to an eastward shift of the SPCZ, which suppressed the rain-bearing convective weather systems associated with both types of La Niña events. Another study attributed strong rainfall anomalies over southeast Queensland during the 2010/11 La Niña event to a change from a pIPO to a nIPO phase (Cai and van Rensch 2012). Further, in December, anomalously warm local SSTs north of Australia compounded the typically wet conditions seen during the same La Niña, leading to the extreme rainfall event in 2010/11 (Evans and Boyer-Souchet 2012). Our analysis shows a contrast in AUMR anomalies during CP La Niña events between IPO phases for northern Australia. December is the key month for the enhanced rainfall during CP La Niña events in nIPO phases (Fig. 6c). The corresponding local SSTa are significantly warm to the NE of Australia, stretching in a southeasterly direction (not shown). Strong and significant moisture flux convergence is found over a similar

region (Fig. 8h), slightly north of these significantly positive SSTa, where the SST gradient is large. This indicates the SPCZ position, which is located approximately over the region with the maximum SST gradient (Folland et al. 2002). These anomalously warm SSTs in the SPCZ region were only observed in December, which may explain the strong moisture flux convergence and positive AUMR anomalies during this month (for CP La Niña events in nIPO periods). In contrast, in pIPO phases for the same month and ENSO event type (December, CP La Niña), the SSTa are weakly positive north of Australia (not shown), and the region with anomalous convergence is located farther north (Fig. 8f). Given the above, the strong positive AUMR and moisture flux convergence anomalies for December during CP La Niña events in nIPO phases (Fig. 8h) are consistent with a southwestward shift of the center of convergence associated with the SPCZ that takes place during La Niña events in nIPO phases (e.g., Folland et al. 2002). This occurs in the month with the warmest local SSTa northeast of Australia and the strongest SST gradient in the southern tropical/subtropical Pacific.

d. CP and EP La Niña in nIPO periods

Expanding on Song et al. (2017), our results highlight a more substantial impact of CP La Niña events than EP La Niña events on AUMR; this applies particularly to NE Australia and nIPO phases. The significant 850-hPa wind anomalies over Australia during CP events in their study support our nIPO phase results in Fig. 7g. In contrast, the Song et al. (2017) EP wind composites show some similarities in the central Pacific and the equatorial Indian Ocean but are more difficult to compare to our results as fewer vectors are shown (less significance). The use of a different dataset (NCEP–NCAR reanalysis) and climatological period (1961–90) and a shorter total analyzed time period in their study can also lead to slight differences in the results. EP events are subject to greater uncertainties associated with AUMR and the related circulation patterns during EP events, with so few occurring in total.

A comparison of CP and EP La Niña events during December in nIPO phases shows that SSTa during EP events are negative to the north and NW of Australia and climatological to the NE (data not shown). In addition to a much weaker large-scale teleconnection between the Indo-Australian region and the central Pacific during EP than CP La Niña events in nIPO periods (see supplemental Fig. 10), the much cooler local SSTa during EP than CP La Niña events may help explain the weak and even negative rainfall anomalies over NE Australia during the EP La Niña events in December.

e. Absolute SSTs

Absolute SSTs were analyzed for both types of CP ENSO events due to the potential of warm SSTa north of Australia to enhance convection and rainfall anomalies over NE Australia (Evans and Boyer-Souchet 2012). Additionally, a large SST gradient can indicate the approximate location of the SPCZ (Folland et al. 2002). However, absolute SSTs (see supplemental Fig. 8) do not show any strong differences in the location of tropical SST maxima or SST gradients between pIPO and nIPO phases for the examined CP ENSO events. Therefore further analysis using climate models is required to assess the causes for the circulation and moisture flux anomalies (e.g., Taschetto et al. 2010a).

f. Decadal ENSO–AUMR teleconnection changes

From the first to the most recent nIPO epoch, the correlations between SSTa and AUMR have weakened over the eastern tropical Pacific. In contrast, the correlations with the central-western Pacific remain strong and significant (Fig. 3). These findings are supported by the AUMR–ENSO index correlations, which show an increase in the correlations with the CP index and a decrease in the correlations with the EP index (Table 2). This change is possibly related to the increased SST variability in the central Pacific since the late 1970s (Wang et al. 2019), including a more frequent occurrence of CP El Niño events relative to several centuries before the commencement of instrumental records (Freund et al. 2019). The westward shift seemed to have only influenced the CP ENSO–AUMR teleconnection in nIPO epochs, during which the correlations are generally stronger. This result agrees with Ashok et al. (2014), who showed that the AUMR–central Pacific SST relationship has strengthened since the late 1970s.

The future development of ENSO diversity is uncertain, though, as found in a recent study by Freund et al. (2020) examining climate simulations from phases 5 and 6 of the Coupled Model Intercomparison Projects (CMIP5 and CMIP6). Changes in future El Niño events may depend on the IPO and long-term warming trends (Freund et al. 2020), which are themselves affected by the IPO (Meehl et al. 2016). However, the representation of the IPO in CMIP5 coupled climate models is subject to strong biases such as weak decadal variability and an incorrect number of simulated IPO phases (Henley et al. 2017; Mann et al. 2020). It also remains a challenge to know if the IPO phase, which modifies the position of the Walker circulation and the teleconnection between the AUMR and ENSO, is responsible for the stronger influence of CP ENSO events on AUMR during nIPO phases. Alternatively, the IPO is itself likely to be influenced by ENSO event type and frequency changes. The lack of accurate characterization of decadal mechanisms in climate models impedes the dynamical link between interannual and decadal variability (Henley et al. 2017; Mann et al. 2020). Such a major challenge requires future research to be adequately addressed (Power et al. 2021).

5. Conclusions

This study has clarified the relationship between IPO phases and ENSO impacts on AUMR. The differences between these impacts during IPO positive and negative phases are greatest for CP ENSO events. The contrast between CP ENSO impacts during positive and negative IPO phases is the most stark. This difference primarily occurs

through a large-scale atmospheric circulation response to an anomalous SST forcing in the central Pacific that is either reinforced or dampened by the underlying decadal background state. The atmospheric response includes variations in moisture fluxes over northern Australia and the Maritime Continent.

As speculated previously (Power et al. 1999), accurate knowledge of the IPO phase could be a source for better predictability (and the likelihood of persistence) of anomalously wet or dry conditions over northern Australia during ENSO events in the future. However, the extent to which the IPO is predictable is not clear (Power et al. 2006, 2021). In fact, it seems to be largely, though not entirely, driven by random changes in ENSO activity (Power et al. 2006, 2021). If the IPO is persistent over many years, then a purported recent shift to a pIPO phase suggests the possibility of weaker large-scale atmospheric circulation anomalies around the Maritime Continent and equatorial Pacific during future CP ENSO events than would be expected if the IPO remained in its negative phase. It also suggests a possible tendency toward below-average AUMR; however, the presence of neutral and negative unfiltered TPI anomalies from around mid-2016 to mid-2021 (www.psl.noaa.gov/data/timeseries/IPOTPI) highlights the importance of not relying on short-term tendencies.

The results presented here suggest that the relationship between AUMR and the CP index is constantly changing. This evolving relationship is demonstrated by the stronger teleconnection in the recent nIPO epoch and may be related to the increasing number of CP El Niño events since the late 1970s (Freund et al. 2019). Furthermore, this strengthening may have only occurred in the nIPO epoch due to the stronger teleconnection between CP ENSO events and AUMR during nIPO than during pIPO phases. We plan to further explore the mechanisms linking decadal and interannual SST variations and northern Australian rainfall using coupled climate models.

Acknowledgments. This research was supported by the Northern Australia Climate Program funded by the Meat and Livestock Australia Donor Company, the Queensland Government's Drought and Climate Adaptation Program, and the University of Southern Queensland, as well as the DeRISK International Climate Initiative. The analysis was conducted using the University of Southern Queensland Fawkes HPC, co-sponsored by the Queensland Cyber Infrastructure Foundation. The climate data toolbox for MATLAB (Greene et al. 2019) aided with displaying the data. We thank Mandy Freund for helpful correspondence in the early stages of the data analysis and also thank the three anonymous reviewers and Chris Folland for their insightful comments to improve the manuscript. We further thank Scott Power for his helpful feedback on the final version of the manuscript.

Data availability statement. HadISST SST data are available through the U.K. Met Office on https://www.metoffice.gov.uk/hadobs/hadisst/data/download.html. 20CRv3 data are available through NOAA on https://psl.noaa.gov/data/gridded/data.20thC_ReanV3.html. AWAP rainfall data is available through the Australian Bureau of Meteorology.

REFERENCES

Ashok, K., S. K. Behera, S. A. Rao, H. Weng, and T. Yamagata, 2007: El Niño Modoki and its possible teleconnection. *J. Geophys. Res.*, **112**, C11007, https://doi.org/10.1029/2006JC003798.

——, C. Nagaraju, A. Sen Gupta, and D. S. Pai, 2014: Decadal changes in the relationship between the Indian and Australian summer monsoons. *Climate Dyn.*, **42**, 1043–1052, https://doi.org/10.1007/s00382-012-1625-4.

Benjamini, Y., and Y. Hochberg, 1995: Controlling the false discovery rate: A practical and powerful approach to multiple testing. *J. Roy. Stat. Soc.*, **57**, 289–300, https://doi.org/10.1111/j.2517-6161.1995.tb02031.x.

Boschat, G., I. Simmonds, A. Purich, T. Cowan, and A. B. Pezza, 2016: On the use of composite analyses to form physical hypotheses: An example from heat wave–SST associations. *Sci. Rep.*, **6**, 29599, https://doi.org/10.1038/srep29599.

Bowman, D. M. J. S., 2002: The Australian summer monsoon: A biogeographic perspective. *Aust. Geogr. Stud.*, **40**, 261–277, https://doi.org/10.1111/1467-8470.00179.

Brown, J. R., A. F. Moise, R. Colman, and H. Zhang, 2016: Will a warmer world mean a wetter or drier Australian monsoon? *J. Climate*, **29**, 4577–4596, https://doi.org/10.1175/JCLI-D-15-0695.1.

Cai, W., and T. Cowan, 2009: La Niña Modoki impacts Australia autumn rainfall variability. *Geophys. Res. Lett.*, **36**, L12805, https://doi.org/10.1029/2009GL037885.

——, and P. van Rensch, 2012: The 2011 southeast Queensland extreme summer rainfall: A confirmation of a negative Pacific decadal oscillation phase? *Geophys. Res. Lett.*, **39**, L08702, https://doi.org/10.1029/2011GL050820.

——, ——, T. Cowan, and A. Sullivan, 2010: Asymmetry in ENSO teleconnection with regional rainfall, its multidecadal variability, and impact. *J. Climate*, **23**, 4944–4955, https://doi.org/10.1175/2010JCLI3501.1.

Capotondi, A., and Coauthors, 2015: Understanding ENSO diversity. *Bull. Amer. Meteor. Soc.*, **96**, 921–938, https://doi.org/10.1175/BAMS-D-13-00117.1.

Carvalho, L. M. V., 2020: Assessing precipitation trends in the Americas with historical data: A review. *Wiley Interdiscip. Rev.: Climate Change*, **11**, e627, https://doi.org/10.1002/wcc.627.

Choi, K.-S., H.-D. Kim, and S.-D. Kang, 2016: Interdecadal variation of Australian summer monsoon during late 1990s. *Int. J. Climatol.*, **36**, 1917–1927, https://doi.org/10.1002/joc.4469.

Chung, C. T. Y., and S. B. Power, 2017: The non-linear impact of El Niño, La Niña and the Southern Oscillation on seasonal and regional Australian precipitation. *J. South. Hemisphere Earth Syst. Sci.*, **67**, 25–45, https://doi.org/10.22499/3.6701.003.

Clark, S., M. J. Reeder, and C. Jakob, 2018: Rainfall regimes over northwestern Australia. *Quart. J. Roy. Meteor. Soc.*, **144**, 458–467, https://doi.org/10.1002/qj.3217.

Cobon, D. H., G. S. Stone, J. O. Carter, J. C. Scanlan, N. R. Toombs, X. Zhang, J. Willcocks, and G. M. McKeon, 2009: The climate change risk management matrix for the grazing industry of northern Australia. *Rangeland J.*, **31**, 31–49, https://doi.org/10.1071/RJ08069.

Conway, D., A. Pereschino, S. Ardoin-Bardin, H. Hamandawana, C. Dieulin, and G. Mahé, 2009: Rainfall and water resources variability in sub-Saharan Africa during the twentieth century. *J. Hydrometeor.*, **10**, 41–59, https://doi.org/10.1175/2008JHM1004.1.

Davidson, N. E., J. L. McBride, and B. J. McAvaney, 1983: The onset of the Australian monsoon during winter MONEX: Synoptic aspects. *Mon. Wea. Rev.*, **111**, 496–516, https://doi.org/10.1175/1520-0493(1983)111<0496:TOOTAM>2.0.CO;2.

Dey, R., S. C. Lewis, and N. J. Abram, 2019a: Investigating observed northwest Australian rainfall trends in Coupled Model Intercomparison Project phase 5 detection and attribution experiments. *Int. J. Climatol.*, **39**, 112–127, https://doi.org/10.1002/joc.5788.

——, ——, J. M. Arblaster, and N. J. Abram, 2019b: A review of past and projected changes in Australia's rainfall. *Wiley Interdiscip. Rev.: Climate Change*, **10**, e577, https://doi.org/10.1002/wcc.577.

Drosdowsky, W., 1996: Variability of the Australian summer monsoon at Darwin: 1957–1992. *J. Climate*, **9**, 85–96, https://doi.org/10.1175/1520-0442(1996)009<0085:VOTASM>2.0.CO;2.

Evans, J. P., and I. Boyer-Souchet, 2012: Local sea surface temperatures add to extreme precipitation in northeast Australia during La Niña. *Geophys. Res. Lett.*, **39**, L10803, https://doi.org/10.1029/2012GL052014.

Evans, S., R. Marchand, and T. Ackerman, 2014: Variability of the Australian monsoon and precipitation trends at Darwin. *J. Climate*, **27**, 8487–8500, https://doi.org/10.1175/JCLI-D-13-00422.1.

Folland, C. K., J. A. Renwick, M. J. Salinger, and A. B. Mullan, 2002: Relative influences of the Interdecadal Pacific Oscillation and ENSO on the South Pacific convergence zone. *Geophys. Res. Lett.*, **29**, 1643, https://doi.org/10.1029/2001GL014201.

Freund, M., B. J. Henley, D. J. Karoly, K. J. Allen, and P. J. Baker, 2017: Multi-century cool and warm season rainfall reconstructions for Australia's major climatic regions. *Climate Past Discuss.*, **13**, 1751–1770, https://doi.org/10.5194/cp-13-1751-2017.

——, ——, ——, H. V. McGregor, N. J. Abram, and D. Dommenget, 2019: Higher frequency of Central Pacific El Niño events in recent decades relative to past centuries. *Nat. Geosci.*, **12**, 450–455, https://doi.org/10.1038/s41561-019-0353-3.

——, J. R. Brown, B. J. Henley, D. J. Karoly, and J. N. Brown, 2020: Warming patterns affect El Niño diversity in CMIP5 and CMIP6 models. *J. Climate*, **33**, 8237–8260, https://doi.org/10.1175/JCLI-D-19-0890.1.

——, A. G. Marshall, M. C. Wheeler, and J. N. Brown, 2021: Central Pacific El Niño as a precursor to summer drought-breaking rainfall over southeastern Australia. *Geophys. Res. Lett.*, **48**, e2020GL091131, https://doi.org/10.1029/2020GL091131.

Greene, C. A., and Coauthors, 2019: The climate data toolbox for MATLAB. *Geochem. Geophys. Geosyst.*, **20**, 3774–3781, https://doi.org/10.1029/2019GC008392.

Henley, B. J., J. Gergis, D. J. Karoly, S. Power, J. Kennedy, and C. K. Folland, 2015: A tripole index for the Interdecadal Pacific Oscillation. *Climate Dyn.*, **45**, 3077–3090, https://doi.org/10.1007/s00382-015-2525-1.

——, and Coauthors, 2017: Spatial and temporal agreement in climate model simulations of the Interdecadal Pacific Oscillation. *Environ. Res. Lett.*, **12**, 044011, https://doi.org/10.1088/1748-9326/aa5cc8.

Hoerling, M. P., A. Kumar, and M. Zhong, 1997: El Nino, La Nina, and the nonlinearity of their teleconnections. *J. Climate*, **10**, 1769–1786, https://doi.org/10.1175/1520-0442(1997)010<1769:ENOLNA>2.0.CO;2.

Holland, G. J., 1986: Interannual variability of the Australian summer monsoon at Darwin: 1952–82. *Mon. Wea. Rev.*, **114**, 594–604, https://doi.org/10.1175/1520-0493(1986)114<0594:IVOTAS>2.0.CO;2.

Jones, D. A., W. Wang, and R. Fawcett, 2009: High-quality spatial climate data-sets for Australia. *Aust. Meteor. Oceanogr. J.*, **58**, 233–248, https://doi.org/10.22499/2.5804.003.

Kajikawa, Y., B. Wang, and J. Yang, 2010: A multi-time scale Australian monsoon index. *Int. J. Climatol.*, **30**, 1114–1120, https://doi.org/10.1002/joc.1955.

Kayano, M. T., R. V. Andreoli, and R. A. F. de Souza, 2020: Pacific and Atlantic multidecadal variability relations to the El Niño events and their effects on the South American rainfall. *Int. J. Climatol.*, **40**, 2183–2200, https://doi.org/10.1002/joc.6326.

Klingaman, N. P., S. J. Woolnough, and J. Syktus, 2013: On the drivers of inter-annual and decadal rainfall variability in Queensland, Australia. *Int. J. Climatol.*, **33**, 2413–2430, https://doi.org/10.1002/joc.3593.

Kug, J. S., and Y. G. Ham, 2011: Are there two types of La Nina? *Geophys. Res. Lett.*, **38**, L16704, https://doi.org/10.1029/2011GL048237.

Kumar, K. K., B. Rajagopalan, M. Hoerling, G. Bates, and M. Cane, 2006: Unraveling the mystery of Indian monsoon failure during El Niño. *Science*, **314**, 115–119, https://doi.org/10.1126/science.1131152.

Li, X. F., J. Yu, and Y. Li, 2013: Recent summer rainfall increase and surface cooling over northern Australia since the late 1970s: A response to warming in the tropical western Pacific. *J. Climate*, **26**, 7221–7239, https://doi.org/10.1175/JCLI-D-12-00786.1.

Lilliefors, H. W., 1967: On the Kolmogorov–Smirnov test for normality with mean and variance unknown. *J. Amer. Stat. Assoc.*, **62**, 399–402, https://doi.org/10.1080/01621459.1967.10482916.

Lin, Z., and Y. Li, 2012: Remote influence of the tropical Atlantic on the variability and trend in North West Australia summer rainfall. *J. Climate*, **25**, 2408–2420, https://doi.org/10.1175/JCLI-D-11-00020.1.

Lu, Z., S. Peng, I. Slette, G. Cheng, X. Li, and A. Chen, 2021: Soil moisture seasonality alters vegetation response to drought in the Mongolian Plateau. *Environ. Res. Lett.*, **16**, 014050, https://doi.org/10.1088/1748-9326/abd1a2.

Mann, M. E., B. A. Steinman, and S. K. Miller, 2020: Absence of internal multidecadal and interdecadal oscillations in climate model simulations. *Nat. Commun.*, **11**, 49, https://doi.org/10.1038/s41467-019-13823-w.

Mantua, N. J., and S. R. Hare, 2002: The Pacific decadal oscillation. *J. Oceanogr.*, **58**, 35–44, https://doi.org/10.1023/A:1015820616384.

McGregor, G., and S. Nieuwolt, 1998: Seasonal variations in regional circulation systems: The monsoons. *Tropical Climatology: An Introduction to the Climates of the Low Latitudes*, Wiley, 119–141.

Meehl, G. A., and J. M. Arblaster, 2011: Decadal variability of Asian-Australian monsoon–ENSO–TBO relationships. *J. Climate*, **24**, 4925–4940, https://doi.org/10.1175/2011JCLI4015.1.

——, A. Hu, and H. Teng, 2016: Initialized decadal prediction for transition to positive phase of the Interdecadal Pacific Oscillation. *Nat. Commun.*, **7**, 11718, https://doi.org/10.1038/ncomms11718.

——, J. M. Arblaster, C. T. Y. Chung, M. M. Holland, A. DuVivier, L. A. Thompson, D. Yang, and C. M. Bitz, 2019: Sustained ocean changes contributed to sudden Antarctic sea ice

retreat in late 2016. *Nat. Commun.*, **10**, 14, https://doi.org/10.1038/s41467-018-07865-9.

Mehta, V. M., C. L. Knutson, N. J. Rosenberg, J. R. Olsen, N. A. Wall, T. K. Bernadt, and M. J. Hayes, 2013: Decadal climate information needs of stakeholders for decision support in water and agriculture production sectors: A case study in the Missouri River basin. *Wea. Climate Soc.*, **5**, 27–42, https://doi.org/10.1175/WCAS-D-11-00063.1.

Nicholls, N., J. L. McBride, and R. J. Ormerod, 1982: On predicting the onset of the Australian wet season at Darwin. *Mon. Wea. Rev.*, **110**, 14–17, https://doi.org/10.1175/1520-0493(1982)110<0014:OPTOOT>2.0.CO;2.

Power, S., T. Casey, C. Folland, A. Colman, and V. Mehta, 1999: Inter-decadal modulation of the impact of ENSO on Australia. *Climate Dyn.*, **15**, 319–324, https://doi.org/10.1007/s003820050284.

——, M. Haylock, R. Colman, and X. Wang, 2006: The predictability of interdecadal changes in ENSO activity and ENSO teleconnections. *J. Climate*, **19**, 4755–4771, https://doi.org/10.1175/JCLI3868.1.

——, and Coauthors, 2021: Decadal climate variability in the tropical Pacific: Characteristics, causes, predictability, and prospects. *Science*, **374**, eaay9165, https://doi.org/10.1126/science.aay9165.

Rasmusson, E. M., and T. H. Carpenter, 1982: Variations in tropical sea surface temperature and surface wind fields associated with the Southern Oscillation/El Niño. *Mon. Wea. Rev.*, **110**, 354–384, https://doi.org/10.1175/1520-0493(1982)110<0354:VITSST>2.0.CO;2.

Rayner, N. A., D. E. Parker, E. B. Horton, C. K. Folland, L. V. Alexander, D. P. Rowell, E. C. Kent, and A. Kaplan, 2003: Global analysis of sea surface temperature, sea ice, and night marine air temperature since the late nineteenth century. *J. Geophys. Res.*, **108**, 4407, https://doi.org/10.1029/2002JD002670.

Ren, H.-L., and F.-F. Jin, 2011: Niño indices for two types of ENSO. *Geophys. Res. Lett.*, **38**, L04704, https://doi.org/10.1029/2010GL046031.

Risbey, J. S., M. J. Pook, P. C. McIntosh, M. C. Wheeler, and H. Hendon, 2009: On the remote drivers of rainfall variability in Australia. *Mon. Wea. Rev.*, **137**, 3233–3253, https://doi.org/10.1175/2009MWR2861.1.

Rodríguez-Fonseca, B., and Coauthors, 2015: Variability and predictability of West African droughts: A review on the role of sea surface temperature anomalies. *J. Climate*, **28**, 4034–4060, https://doi.org/10.1175/JCLI-D-14-00130.1.

Rotstayn, L. D., S. J. Jeffrey, M. A. Collier, S. M. Dravitzki, A. C. Hirst, J. I. Syktus, and K. K. Wong, 2012: Aerosol- and greenhouse gas-induced changes in summer rainfall and circulation in the Australasian region: A study using single-forcing climate simulations. *Atmos. Chem. Phys.*, **12**, 6377–6404, https://doi.org/10.5194/acp-12-6377-2012.

Roxy, M. K., P. Dasgupta, M. J. McPhaden, T. Suematsu, C. Zhang, and D. Kim, 2019: Twofold expansion of the Indo-Pacific warm pool warps the MJO life cycle. *Nature*, **575**, 647–651, https://doi.org/10.1038/s41586-019-1764-4.

Sekizawa, S., H. Nakamura, and Y. Kosaka, 2018: Interannual variability of the Australian summer monsoon system internally sustained through wind-evaporation feedback. *Geophys. Res. Lett.*, **45**, 7748–7755, https://doi.org/10.1029/2018GL078536.

Sharmila, S., and H. H. Hendon, 2020: Mechanisms of multiyear variations of Northern Australia wet-season rainfall. *Sci. Rep.*, **10**, 5086, https://doi.org/10.1038/s41598-020-61482-5.

Si, D., and Y. Ding, 2016: Oceanic forcings of the interdecadal variability in East Asian summer rainfall. *J. Climate*, **29**, 7633–7649, https://doi.org/10.1175/JCLI-D-15-0792.1.

Slivinski, L. C., and Coauthors, 2019: Towards a more reliable historical reanalysis: Improvements for version 3 of the Twentieth Century Reanalysis system. *Quart. J. Roy. Meteor. Soc.*, **145**, 2876–2908, https://doi.org/10.1002/qj.3598.

Song, L., S. Chen, W. Chen, and X. Chen, 2017: Distinct impacts of two types of La Niña events on Australian summer rainfall. *Int. J. Climatol.*, **37**, 2532–2544, https://doi.org/10.1002/joc.4863.

Srivastava, A., M. Pradhan, B. N. Goswami, and S. A. Rao, 2019: Regime shift of Indian summer monsoon rainfall to a persistent arid state: External forcing versus internal variability. *Meteor. Atmos. Phys.*, **131**, 211–224, https://doi.org/10.1007/s00703-017-0565-2.

Stuecker, M. F., F.-F. Jin, A. Timmermann, and S. McGregor, 2015: Combination mode dynamics of the anomalous northwest Pacific anticyclone. *J. Climate*, **28**, 1093–1111, https://doi.org/10.1175/JCLI-D-14-00225.1.

Suppiah, R., 1992: The Australian summer monsoon: A review. *Prog. Phys. Geogr.*, **16**, 283–318, https://doi.org/10.1177/030913339201600302.

Takahashi, K., A. Montecinos, K. Goubanova, and B. Dewitte, 2011: ENSO regimes: Reinterpreting the canonical and Modoki El Niño. *Geophys. Res. Lett.*, **38**, L10704, https://doi.org/10.1029/2011GL047364.

Taschetto, A. S., C. C. Ummenhofer, A. S. Gupta, and M. H. England, 2009: Effect of anomalous warming in the central Pacific on the Australian monsoon. *Geophys. Res. Lett.*, **36**, L12704, https://doi.org/10.1029/2009GL038416.

——, R. J. Haarsma, A. S. Gupta, C. C. Ummenhofer, K. J. Hill, and M. H. England, 2010a: Australian monsoon variability driven by a Gill–Matsuno-type response to central west Pacific warming. *J. Climate*, **23**, 4717–4736, https://doi.org/10.1175/2010JCLI3474.1.

——, ——, A. Sen Gupta, C. C. Ummenhofer, and M. H. England, 2010b: Teleconnections associated with the intensification of the Australian monsoon during El Niño Modoki events. *IOP Conf. Ser. Earth Environ. Sci.*, **11**, 012031, https://doi.org/10.1088/1755-1315/11/1/012031.

——, A. Sen Gupta, H. H. Hendon, C. C. Ummenhofer, and M. H. England, 2011: The contribution of Indian Ocean sea surface temperature anomalies on Australian summer rainfall during El Niño events. *J. Climate*, **24**, 3734–3747, https://doi.org/10.1175/2011JCLI3885.1.

Terray, P., P. Delecluse, S. Labattu, and L. Terray, 2003: Sea surface temperature associations with the late Indian summer monsoon. *Climate Dyn.*, **21**, 593–618, https://doi.org/10.1007/s00382-003-0354-0.

Timmermann, A., and Coauthors, 2018: El Niño–Southern Oscillation complexity. *Nature*, **559**, 535–545, https://doi.org/10.1038/s41586-018-0252-6.

Trenberth, K. E., and D. P. Stepaniak, 2001: Indices of El Niño evolution. *J. Climate*, **14**, 1697–1701, https://doi.org/10.1175/1520-0442(2001)014<1697:LIOENO>2.0.CO;2.

Ventura, V., C. J. Paciorek, and J. S. Risbey, 2004: Controlling the proportion of falsely rejected hypotheses when conducting multiple tests with climatological data. *J. Climate*, **17**, 4343–4356, https://doi.org/10.1175/3199.1.

Wang, B., X. Luo, Y. Yang, W. Sun, M. A. Cane, W. Cai, S. Yeh, and J. Liu, 2019: Historical change of El Niño properties sheds light on future changes of extreme El Niño. *Proc. Natl. Acad. Sci. USA*, **116**, 22 512–22 517, https://doi.org/10.1073/pnas.1911130116.

Wang, P. X., B. Wang, H. Cheng, J. Fasullo, Z. T. Guo, T. Kiefer, and Z. Y. Liu, 2017: The global monsoon across time scales: Mechanisms and outstanding issues. *Earth-Sci. Rev.*, **174**, 84–121, https://doi.org/10.1016/j.earscirev.2017.07.006.

Webster, P. J., V. O. Magaña, T. N. Palmer, J. Shukla, R. A. Tomas, M. Yanai, and T. Yasunari, 1998: Monsoons: Processes, predictability, and the prospects for prediction. *J. Geophys. Res.*, **103**, 14 451–14 510, https://doi.org/10.1029/97JC02719.

Wilks, D. S., 2011: *Statistical Methods in the Atmospheric Sciences.* 3rd ed. Academic Press, 704 pp.

Yeh, S. W., J. S. Kug, B. Dewitte, M. H. Kwon, B. P. Kirtman, and F.-F. Jin, 2009: El Niño in a changing climate. *Nature*, **461**, 511–514, https://doi.org/10.1038/nature08316.

Yuan, Y., and S. Yang, 2012: Impacts of different types of El Niño on the East Asian climate: Focus on ENSO cycles. *J. Climate*, **25**, 7702–7722, https://doi.org/10.1175/JCLI-D-11-00576.1.

Zhou, T., R. Yu, H. Li, and B. Wang, 2008: Ocean forcing to changes in global monsoon precipitation over the recent half-century. *J. Climate*, **21**, 3833–3852, https://doi.org/10.1175/2008JCLI2067.1.